

Aus dem Fachbereich Medizin  
der Johann Wolfgang Goethe-Universität  
Frankfurt am Main

betreut am  
Zentrum der Psychischen Gesundheit  
Klinik für Psychiatrie, Psychosomatik und Psychotherapie  
Direktor: Prof. Dr. Andreas Reif

**Improved correspondence of fMRI visual field localizer data  
after cortex-based macroanatomical alignment**

Dissertation  
zur Erlangung des Doktorgrades der Medizin  
des Fachbereichs Medizin  
der Johann Wolfgang-Goethe-Universität  
Frankfurt am Main

vorgelegt von  
Mishal Qubad

aus Kabul, Afghanistan

Frankfurt am Main, 2022

Dekan:	Prof. Dr. Stefan Zeuzem
Referent:	Prof. Dr. Andreas Reif
Korreferent:	Prof. Dr. Stefan Weidauer
Tag der mündlichen Prüfung:	29.03.2023

*Für meinen Vater.*

## **Inhaltsverzeichnis**

Zusammenfassung (Englisch) .....	5
Zusammenfassung (Deutsch) .....	7
Abkürzungsverzeichnis .....	9
Übergreifende Zusammenfassung .....	10
The visual system .....	10
Visual mapping techniques .....	10
Interindividual macroanatomical variability.....	11
Approaches to address interindividual macroanatomical variability .....	12
The present research project.....	13
Discussion .....	16
Übersicht der Publikation .....	20
Publikation.....	21
Darstellung des eigenen Anteils an der Publikation (Confirmation of contributions).....	42
Literaturverzeichnis .....	43
Schriftliche Erklärung .....	50
Danksagung .....	51

## Zusammenfassung (Englisch)

The visual system encompasses about 20% of the cerebral cortex<sup>1</sup> and plays a pivotal role in higher-order cognitive processes such as attention and working memory.<sup>2-4</sup> Cognitive impairments constitute a central role in neuropsychiatric disorders such as schizophrenia (SZ).<sup>5-9</sup> Impairments are described in visual perceptual processes including contrast, and emotion discrimination as well as in the ability to identify visual irregularities and in higher-order cognition like visual attention and working memory.<sup>10-18</sup> Furthermore, perceptual and higher-order cognitive processes are part of the Research Domain Criteria (RDoC) project that aims to develop dimensional and transdiagnostic constructs with defined links to specific brain circuits.<sup>19,20</sup> Therefore, the detailed study of the visual system using functional magnetic resonance imaging (fMRI) is essential to understand the processes in healthy individuals but also in populations with neuropsychiatric disorders.

Visual mapping techniques include functional localizer tasks to map functionally defined regions like the fusiform face area (FFA), retinotopic mapping to map specific brain regions that are retinotopically organized in full, and visual-field localizer paradigms to define circumscribed areas within retinotopically organized areas.<sup>1,21-26</sup> Thus, the latter allow studying local information processing in early visual areas. Despite advances in neuroimaging techniques, analyses of fMRI data at the group-level are impeded by interindividual macroanatomical variability. This reduces the reliability to accurately define visual areas particularly at the group-level and decreases statistical power.<sup>25,27-34</sup> Single-subject based solutions for this problem are not appropriate.<sup>35</sup> Analyses after volume-based alignment (VBA)<sup>27,36-39</sup> and primary surface-based analyses without macroanatomical alignment<sup>30,40-44</sup> do not increase macroanatomical correspondence sufficiently. Cortex-based alignment (CBA) approaches are recommended as an alternative technique to address this obstacle.<sup>41</sup> However, CBA has not been evaluated for visual-field localizer paradigms. Therefore, we aimed to evaluate potential benefits of CBA for an attention-enhanced visual field localizer paradigm that maps circumscribed regions in retinotopically organized visual areas. Since previous studies solely compared surface-based data before and after CBA,<sup>25</sup> we aimed to compare all three techniques: (1) a volume-based

alignment (VBA), (2) a surface-based data set without (SBAV) and (3) a surface-based data set with macroanatomical alignment (CBA). Furthermore, we sought to define regions of interest (ROI) that subsequently can be used for the study of higher-order cognitive processes. Also, we aimed to investigate whether CBA facilitates the study of functional asymmetries in early visual areas as these were described in previous studies. Healthy volunteers (n=50) underwent fMRI in a 3-Tesla Siemens Trio scanner while performing an attention-enhanced visual field localizer paradigm. Our task consisted of a series of flickering, black-and white colored checkerboard stimuli that randomly appeared at one of four locations comprising the participants' visual quadrants. In 25% of the trials the centrally located squares briefly changed their color to yellow (target trial). Participants had to indicate detection of a target by button press. Data analysis was conducted using Brain Voyager 20.6.<sup>45</sup> Our approach for macroanatomical alignment included a high-resolution, multiscale curvature driven alignment procedure minimizing interindividual macroanatomical variability. Here, each folding pattern was aligned to a dynamically updated group average. Thus, we counteracted a possible confounding effect of a suboptimal selection of an individual target brain with a folding pattern deviating considerably from the cohort average. Group ROIs after CBA showed increased spatial consistency, vertical symmetry, and an increase of size. This was corroborated by an increase in the probability of activation overlap of up to 86%. CBA increased macroanatomical correspondence and thus ameliorated results of multi-subject ROI analyses. Functional differences in the form of a downward bias in visual hemifields were measured with increased reliability. In summary, our findings provide clear evidence for the superiority of CBA for the study of local information processing in early visual cortex at the group-level. This approach is of relevance for the study of visual dysfunction in neuropsychiatric disorders including schizophrenia as they show impaired visual processing that in turn impacts higher-order cognitive processes and in consequence functional outcome.<sup>46, 47</sup> In addition, our attention-enhanced visual field localizer paradigm will be useful for machine learning approaches such as multivariate pattern analysis decoding local information processes and connectivity patterns.

## Zusammenfassung (Deutsch)

Das visuelle System umfasst ca. 20% des zerebralen Kortex<sup>1</sup> und spielt eine bedeutende Rolle in Aufmerksamkeits- sowie Arbeitsgedächtnisprozessen.<sup>2-4</sup> Kognitive Defizite und Defizite im visuellen System sind zudem zentraler Bestandteil neuropsychiatrischer Erkrankungen wie der Schizophrenie.<sup>5-9</sup> Bei Patienten mit Schizophrenie werden z.B. Einschränkungen in der selektiven Aufmerksamkeit sowie in der Fähigkeit Unregelmäßigkeiten, Farben und Kontraste adäquat zu erkennen, beschrieben.<sup>10-17</sup> Diese Beispiele heben die Relevanz eines funktionierenden visuellen Systems sowie die Untersuchung der neurophysiologischen Grundlagen hervor. Befürwortet wird dies auch durch das RDoC-Projekt, welches das Ziel hat, neuropsychiatrische Erkrankungen auf Basis von Defiziten in kognitiven Domänen und neuronalen Netzwerken zu beschreiben.<sup>19, 20</sup> Hierbei wird auch empfohlen, Wahrnehmungsprozesse zu berücksichtigen. Zusammenfassend ist somit die detaillierte Untersuchung des visuellen Systems mittels funktioneller Magnetresonanztomographie (fMRT) essenziell, um die Abläufe in gesunden Personen aber auch in Populationen mit einer neuropsychiatrischen Erkrankung zu verstehen. Im Rahmen solcher Untersuchungen gibt es verschiedene Methoden, die genutzt werden können: die Untersuchung funktionell definierter visueller Areale anhand einer sog. *functional-localizer* Aufgabe, retinotop Kartierung der visuellen Areale, sowie die Untersuchung umschriebener visueller Regionen innerhalb dieser retinotop organisierten Systeme mittels *visual-field-localizer* Aufgaben.<sup>1, 21-26</sup> Letztere ermöglichen insbesondere die Untersuchung lokaler Informationsverarbeitung einfacher visueller Stimuli in frühen visuellen Arealen. All diese Ansätze haben eine limitierende Gemeinsamkeit, und zwar interindividuelle, makroanatomische Unterschiede, die die Analysen auf Gruppenebene erschweren und die statistische Aussagekraft minimieren.<sup>25, 27-34</sup> Als Alternative kann die Anwendung eines kortexbasierten Angleichungsverfahrens (CBA) dienen.<sup>41</sup> Für *visual-field-localizer* Aufgaben ist CBA jedoch noch nicht untersucht. Darüber hinaus beschränkten sich die Untersuchungen bislang primär auf oberflächenbasierte Datenanalysen.<sup>25</sup> Hierbei wurde postuliert, dass oberflächenbasierte Methoden ohne CBA vergleichbar mit strikt volumen-basierten Analysen sind. Ziel unserer Studie war es, Effekte der CBA auf *visual-field-localizer* Aufgaben zu evaluieren

und *ROIs* zu definieren, die auch für die Untersuchung höherer kognitiver Prozesse genutzt werden können. Darüber hinaus beabsichtigten wir, alle drei Methoden miteinander zu vergleichen: (1) volumenbasierte Angleichung (VBA), (2) oberflächenbasierte Angleichung ohne makroanatomische (SBAV) und (3) mit makroanatomischer Angleichung (CBA). Gesunde Kontrollprobanden (n = 50) ohne neuropsychiatrische Erkrankung bearbeiteten im 3-Tesla-fMRT eine *visual-field-localizer* Aufgabe, bestehend aus einer Serie blinkender, runder, schwarz-weiß-gefärbter Schachbrettmuster. Die Muster erschienen zufällig in vier verschiedenen Gesichtsfeldarealen. In 25 % der Fälle änderte sich die Farbe der zwei zentral gelegenen Quadrate kurzzeitig in Gelb (*target trial*). Das Bemerkens der Änderung sollte mittels Tastendrucks zurückgemeldet werden. Alle drei Analyseverfahren (VBA, SBAV, CBA) wurden mit Brain Voyager 20.6 durchgeführt.<sup>45</sup> Grundlage der CBA-Methode sind kortikale Faltungsmuster mit der Besonderheit, dass die Datensätze an ein dynamisch aktualisiertes Zielgehirn angeglichen werden. Hierdurch vermeidet man, ein Zielgehirn mit ausgeprägter Abweichung vom Gruppenschnitt auszuwählen. Wir definierten vier *ROIs* für alle drei Methoden (VBA, SBAV, CBA), um diese miteinander zu vergleichen. CBA verbesserte die räumliche Präzision der Gruppenaktivitätskarten und führte zu deutlich symmetrischer und fokussierter Verteilung der Aktivitätscluster. Bestätigt wurde dies durch eine Zunahme der Überlappungswahrscheinlichkeit der Aktivitätscluster um bis zu 86%. Es zeigte sich somit eine deutliche Verbesserung der Ergebnisse der Gruppenanalyse. Funktionelle Unterschiede in Form von Asymmetrien, die in elektrophysiologischen Untersuchungen beschrieben wurden, konnten hierdurch reliabler dargestellt werden. CBA-basierte Analyseverfahren sind somit für die Untersuchung früher visueller Areale einer volumen-basierten aber auch einer rein oberflächen-basierten Analyse ohne makroanatomische Angleichung überlegen und können daher in Patientengruppen, die eine erhöhte interindividuelle makroanatomische Variabilität aufweisen wie der Schizophrenie, genutzt werden.



## Abkürzungsverzeichnis

AC	Anterior commissure
AI	Asymmetry index
BOLD	Blood-oxygenation-level-dependent
CBA	Cortex-based alignment, kortex-basierte Angleichung
FFA	Fusiform face area
fMRI	Functional magnetic resonance imaging
fMRT	Funktionelle Magnetresonanztomographie
ITI	Intertrial interval
MNI space	Montreal Neurological Institute space
MVPA	Multivariate pattern analysis
PC	Posterior commissure
PDM	Probability difference map
PM	Probability map
RDoC project	Research Domain Criteria project
ROI	Region of interest
SBAV	Surface-based analysis using VBA
SNR	Signal-to-noise-ratio
SZ	Schizophrenia
VBA	Volume-based alignment
WM	Working memory

# Übergreifende Zusammenfassung

## The visual system

The visual system occupies about 20% of the human cerebral cortex<sup>1</sup> and is characterized by a complex and hierarchical organization.<sup>48</sup> It can broadly be divided into two parts consisting of an ophthalmic and neurological. The latter encompasses the occipital cortex containing the primary (V1) and secondary visual areas (V2-V5) and subsequently extends to temporo-parietal regions.<sup>49, 50</sup> Importantly, it shows close interconnections with regions involved in higher-order cognition like visual selective attention and visual working memory (WM).<sup>2-4, 49, 51</sup> Its interaction with areas involved in visual WM processes is also reflected by the sensory recruitment hypothesis<sup>52-55</sup> which proposes neural populations in early visual regions to be involved in the maintenance of visual information via representations in the same early visual area that initially encoded the presented visual information.<sup>53, 54, 56</sup> Such recruitment is commonly initiated by regions involved in higher-order cognition like frontoparietal regions.<sup>53, 54, 56</sup> Importantly, several findings indicate that such recruitment might also account for an increased precision of memory storage.<sup>53</sup>

## Visual mapping techniques

Using fMRI is a common approach to study the visual system with its topographical representations and connectivity patterns to higher-order cognitive areas. Visual mapping techniques include retinotopic mapping and population receptive field mapping,<sup>1, 21, 22</sup> functional localizer paradigms,<sup>1, 22, 57, 58</sup> and finally visual-field localizer paradigms.<sup>26, 59, 60</sup> Functional localizer paradigms allow to map higher-order visual areas like the FFA, extrastriate body area and parahippocampal place area that are specialized in processing complex visual information.<sup>1, 24, 25, 57, 58</sup> In contrast, retinotopic mapping and population receptive field mapping allow delineating early visual areas in full.<sup>1, 21, 22</sup> Finally, visual-field localizer tasks are utilized to define circumscribed regions within a retinotopically organized brain region, thus delineating task-relevant positions in early visual cortex in isolation.<sup>59, 60</sup> To summarize, visual-field localizer paradigms allow studying local information processing within a visual area. For this purpose, the

use of flashing checkerboard stimuli are proposed, as these stimuli cover the exact area of interest within the visual field and lead to strong blood-oxygenation-level-dependent (BOLD) signal increases in early visual areas (V1-V3).<sup>59</sup> Trials with a sudden change of the actual stimulus – that was initially used to map a specific brain region (“non-target”) – are characterized as target trials. Due to its salience, a target stimulus requires the subject to attend to that mismatch, thus enhancing stimulus processing via bottom-up attention,<sup>60-62</sup> and increasing the signal-to-noise-ratio (SNR).<sup>63</sup> Overall, these target trials can induce attentional modulation by task demands which amplifies the BOLD-response<sup>26, 63</sup> and in consequence the reliability of the resulting localizer maps.<sup>63</sup> We refer to these tasks as attention-enhanced visual field localizer paradigms.

### Interindividual macroanatomical variability

Despite advances in neuroimaging and the application of the aforementioned procedures, interindividual macroanatomical variability impedes analysis of fMRI data at the group-level. In particular, specific brain regions can differ both in size and location impairing group-based analyses.<sup>25, 27-34</sup> This variability is the result of divergent cortical folding patterns between individuals. Notably, interindividual macroanatomical variability is evident in V1<sup>29, 64</sup> as well as in extrastriate visual regions.<sup>34</sup> For example, V1 surface area can differ about twofold in size between individuals.<sup>29, 64-67</sup> Importantly, findings from postmortem studies also imply interhemispheric variability of Brodmann areas 17 and 18 within the same individual.<sup>65, 68</sup> In addition, they reported inter- and intraindividual variabilities in sulcal patterns.<sup>65, 68</sup> Additionally, the location of V5 – the visual motion area – can differ about 20 mm between individuals.<sup>68</sup> Consequently, such variability might account for individual differences in visual information processing.<sup>29, 64, 69, 70</sup> For example, previous findings in healthy populations using volume-based fMRI described a downward bias with higher BOLD-response amplitudes to tasks in the lower visual hemifield.<sup>71, 72</sup> Such differences might result from true group differences and true functional variability but also from a biased analysis due to interindividual macroanatomical variability. All in all, this variability limits the reliability to accurately identify specific brain regions like visual areas at the group-level.<sup>25</sup>

## Approaches to address interindividual macroanatomical variability

Group-based analyses necessitate spatial normalization to a standardized three-dimensional (Cartesian) coordinate system like Talairach-space<sup>39</sup> and MNI-space<sup>36</sup> aiming to create a common space for group-based analysis. Talairach transformations employ anatomical landmarks, namely the anterior (AC) and posterior commissure (PC) aiming to create a horizontal plane (AC-PC plane).<sup>39</sup> Based on this plane three axes are defined: x, y, and z running from left-to-right through the AC (x-axis), anterior-to-posterior (y-axis, AC-PC) and superior-to-inferior through the AC (z-axis). These are subsequently utilized to manually outline the outer cortical boundaries by determining the most extreme points of the brain, thus creating a bounding box that runs parallel to the aforementioned axes and specifies the borders of the cerebrum.<sup>39, 73</sup> Alternatively, one can employ a fully data-driven registration of structural images to an average template brain for transformation as implemented for MNI space.<sup>36, 73</sup> Such transformation techniques facilitate comparing signal locations across subjects and studies.<sup>27</sup> However, these traditional stereotactic MRI coordinate systems do not correct interindividual macroanatomical variability.<sup>25</sup> Consequently, specific landmarks can still differ in location across subjects, e.g. the precentral and postcentral gyrus.<sup>25</sup> Pooled single-subject ROIs combined with the overall group-based probability for that ROI at each point in a Cartesian coordinate system can increase functional resolution and sensitivity and is therefore proposed as an alternative approach.<sup>35</sup> However, such an approach is not suitable for studying interactions between visual areas and higher-order cognitive areas at the group-level using whole-brain analyses and it does not reduce macroanatomical variability sufficiently. To summarize, these approaches are referred to as volume-based alignment (VBA) and allow comparing brains across individuals to a certain degree.<sup>36-39</sup> However, they do not take into account topological properties of the cortex and geometric features like sulci and gyri, thus continuing to lack sufficient macroanatomical correspondence.<sup>37, 74</sup> Surface-based techniques on the other hand, allow the use of a geodesic coordinate system with a two-dimensional representation of the cerebral cortex.<sup>30, 40-44</sup> Compared to VBA, surface-based approaches increase the SNR by reducing contamination caused by white matter and cerebrospinal fluid. In addition, these techniques

mostly preclude contamination resulting from cortical regions adjacent in volume space but notably more distant in surface space.<sup>75, 76</sup> Overall, such approaches allow constraining critical data preprocessing steps including spatial smoothing to cortical tissue, thus increasing the SNR by avoiding the above-mentioned contamination.<sup>75</sup> Hence, surface-based methods constitute an important alternative approach. For further improvement of macroanatomical correspondence, information about individual cortical folding patterns can be used to apply a mostly or fully data-driven macroanatomical alignment of the cortex respecting the topography of the cortex to a much larger degree.<sup>30, 40, 42-44, 77</sup> This method is generally categorized as cortex-based alignment (CBA). Hence, CBA is recommended as an alternative alignment technique to mitigate macroanatomical variability.<sup>41</sup> To date, the benefits of CBA have been evaluated for retinotopic mapping<sup>40, 78</sup> and for functional localizer paradigms<sup>24, 25, 79, 80</sup> but not yet for attention-enhanced visual-field localizer paradigms. Additionally, thus far these studies have constrained the comparison of alignment approaches to only surface-based analyses before and after CBA treating the former as a proxy for VBA.<sup>25</sup> However, this might underestimate the full effects of CBA as the differences are limited to macroanatomical alignment while both datasets share the same advantage of an increased SNR. An intermediate approach, that we categorize as “surface-based analysis using VBA” (SBAV), allows evaluating the impact of surface-based analyses in isolation.

### The present research project

Aims: The objective of our study was to evaluate potential benefits of CBA for an attention-enhanced visual field localizer paradigm that maps a circumscribed region in retinotopically organized visual areas. As previous studies primarily compared solely surface-based data before and after CBA, we aimed to compare all three techniques. Moreover, we aimed to define ROIs that are subsequently useful for the study of higher-order cognitive processes. Finally, we sought to investigate whether CBA facilitates the study of functional asymmetries in early visual areas. Methods: Healthy, non-smoking volunteers (n=50) underwent fMRI in a 3T MAGNETOM Trio scanner while performing an attention-enhanced visual field localizer paradigm. The task consisted of a series of flickering, round-

shaped, black-and-white colored checkerboard stimuli (flicker frequency = 7.5 Hz). These stimuli appeared randomly at homologous positions of the participants' visual quadrants for 2000 ms reflecting standard trials. The regular inter-trial-interval (ITI) was 0 ms. However, every 10 to 14 trials, the ITI increased to 2000 ms. For attentional modulation, during 25% of the trials the two centrally located squares turned their color to yellow for 133 ms, thus representing target trials. Participants were required to indicate by button-press the detection of the target while continuously fixating a black, x-shaped fixation cross displayed at the center of the screen. For fMRI data analysis we used Brain Voyager 20.6<sup>45</sup>, the NeuroElf toolbox ([www.neuroelf.net](http://www.neuroelf.net)), R 4.1.2 ([www.r-project.org](http://www.r-project.org)) and custom software written in Matlab 9.10 ([www.mathworks.com](http://www.mathworks.com)). Data analyses comprised structural and functional image pre-processing steps. Structural data pre-processing included background cleaning, brain extraction, bias field correction and transformation into Talairach coordinate space. Subsequently, we employed a segmentation step along the white-and-gray matter boundary as a prerequisite for surface-based analysis steps with and without CBA. This step included the reconstruction of cortical hemispheres into mesh representations that were then transformed into spherical representations. For CBA, we used these spherical representations to apply a high-resolution, multiscale cortex-based alignment procedure based on the individual curvature maps of all participants. This step comprised a rigid and a subsequent non-rigid alignment step.<sup>25, 45</sup> During non-rigid CBA each cortical hemisphere is aligned repetitiously to a dynamically updated group-average following a coarse-to-fine matching strategy to eliminate the possible confound of a static target brain based on an individual brain, whose cortical folding pattern might deviate considerably from the group average.<sup>25</sup> To circumvent a further potential confounding effect of a randomly drawn brain for the initial rigid alignment, we first conducted a preliminary CBA that included both steps. The average brain emerging from this preliminary CBA was then utilized for a second final CBA, again comprising rigid and non-rigid CBA. Functional data pre-processing started in volume space and included slice timing correction, motion correction and echo-planar imaging distortion correction before coregistration to the structural data. Next, we transformed the functional data (VBA, SBAV, CBA) into Talairach coordinate space. For VBA, we continued pre-processing in volume space which included spatial smoothing, linear trend

removal and temporal high-pass filtering. For SBAV and CBA, we continued pre-processing in surface space which included spatial smoothing, linear trend removal and temporal high-pass filtering. Overall, we generated three different functional data sets, i.e., a volume-based data set (VBA), a surface-based data set without (SBAV) and a surface-based data set with macroanatomical alignment (CBA). These datasets were directly compared to one another. For data comparison we identified four ROIs for each dataset while focusing on mapping the areas that were preferentially activated by our attention-enhanced visual field localizer paradigm. Subsequently, using these ROIs we calculated the horizontal and vertical symmetry (also known as asymmetry index, (AI)) for each dataset. In addition, we generated probability maps (PM) and probability difference maps (PDM) for each dataset. The PMs reflect the relative number of subjects showing significant task-related activity in our single-subject analysis, thus allowing the quantification and visualization of the spatial consistency of activation patterns.<sup>81, 82</sup> The calculated PDMs allow to quantify alterations in spatial consistency of these position selective activation patterns. Finally, for CBA and SBAV we determined the peak vertices for each single-subject full ROI and computed the vertex-wise number of peak vertices to estimate the degree of overlap between subjects. This analysis allowed a more direct assessment and visualization of the effects of macroanatomical alignment on the spatial correspondence of single-subject ROIs. Results: CBA led to a considerable improvement of group ROI analyses compared to SBAV and VBA. Overall, in two out of four ROIs we observed a pattern of increasing cluster size. The corresponding average time-courses of each ROI showed clear position selectivity independent of alignment technique. The calculated AIs revealed greater vertical symmetry of both upper and lower visual hemifield ROIs for CBA and VBA compared to SBAV. Regarding horizontal symmetry, the calculated AIs revealed greater horizontal symmetry of both upper and lower visual hemifield ROIs only for CBA. Maximum probability of activation overlap (PM) was located at the center of the defined ROIs for all datasets. For CBA, maximum probability of activation overlap was up to 86% (VBA 55 %, SBAV 66%). Compared to VBA and SBAV datasets, this was accompanied by a decrease in the spread of functional activation around the core ROIs. In the PDMs for CBA minus SBAV, we observed a maximum increase in the probability of activation overlap of 44%

in the central ROIs. This was paralleled by a decrease in the probability of activation overlap of 32% in further peripheral occipital areas. In the PDMs for CBA minus VBA, we observed a maximum increase in the probability of activation overlap of 52%. This was paralleled by a decrease in the probability of activation overlap of 36% in further peripheral areas. Finally, the peak vertex distribution maps and the calculation of the vertex-wise number of peak vertices showed an increase in the number of overlapping peak vertices per vertex for each visual quadrant for CBA compared to SBAV, thus leading to a less spatial variability.

## Discussion

Compared to VBA and SBAV, CBA constitutes a promising approach for facilitating and improving the study of local information processing in early visual areas at the group-level. This was evident in the considerable improvement of our group ROI analyses indicating an enhanced power for CBA to detect subregions of early visual areas. Moreover, our PMs and PDMs illustrated the reduction of spurious activation after CBA. This implies that in contrast to CBA-based group analyses, SBAV and VBA misrepresent the size of visual ROIs, a finding that is also mirrored by changes of the center of gravity of group ROIs between SBAV and CBA. The decrease of variability of single-subject ROI peak vertex locations for each visual quadrant implies the mitigation of macroanatomical and functional inter-subject variability after CBA to be the reason for the improved results at the group-level. Our findings corroborate that SBAV approaches already improve the SNR, but only the CBA technique shows advantages of both an improved SNR and increased macroanatomical correspondence. In addition, this indicates that using SBAV as a proxy for VBA would underestimate the actual benefits of CBA.

Previous findings using volume-based strategies described lateralized effects on neurophysiological parameters in early visual areas.<sup>83, 84</sup> Since the lateralization we first observed for SBAV did not persist after CBA, this raises the question of whether such a lateralization might result partly from poor macroanatomical correspondence rather than actual functional differences.

Moreover, we observed persisting larger group ROIs for the lower visual hemifield. The following explanations are possible regarding these differences



between the upper and lower visual hemifield. On the one hand, higher residual anatomical variability in ventral occipital cortex, representing the upper visual hemifield, might have elicited these findings. This is in line with previous observations of a CBA-based probabilistic atlas of the visual system that showed larger probabilistic ROIs for dorsal V1 and dorsal V2 than for ventral V1 and ventral V2.<sup>24</sup> On the other hand, previous findings also showed differences in receptor densities with higher cone density in the superior parts of the retina processing visual information from lower visual hemifields and higher rod density in the inferior parts of the retina processing visual information from upper visual hemifields.<sup>85, 86</sup> Additionally, dorso-ventral asymmetries in receptor densities in V2 and V3, as well as higher GABA-A and muscarinic M3-receptor density in ventral parts of V2 and V3 have been reported.<sup>86, 87</sup> In sum, these findings might also account for our observed results. Moreover, several reports indicate behavioral advantages in the lower visual hemifield for shape discrimination,<sup>71, 72, 88-90</sup> reflecting differences in the functional architecture of early visual regions. These reports have been attributed to the fact that regions processing visual information from the lower visual hemifield are more closely tied to the dorsal visual pathway, thus indicating that the lower visual hemifields might be more specialized for the localization and representation of space. All in all, these observations illustrate actual differences in functional architecture of early visual areas representing the upper and lower visual hemifield respectively.<sup>90, 91</sup>

The reduction of interindividual macroanatomical variability increases statistical power when studying visual areas at the group-level. This in turn can be utilized in studies focusing on functional and effective connectivity analyses.<sup>92, 93</sup> Moreover, our attention-enhanced visual field localizer paradigm and our ROIs can be used as a basis for multivariate pattern analysis (MVPA).<sup>94, 95</sup> Here, in a first step our ROIs can be utilized to accurately decode activity patterns, i.e., to use information derived from activity patterns to determine which task-related stimulus (“standard stimulus” vs. “target stimulus”) is processed at a specific time-point. Moreover, our findings raise the question of whether MVPA might benefit from CBA when using multi-subject based ROIs. Here, we expect to observe an improved power to accurately decode information due to the increase of the SNR and macroanatomical correspondence. Also, classifiers acquired after MVPA

might serve as functional biomarkers to assess symptom severity,<sup>96</sup> to delineate subgroups of patients,<sup>97</sup> or to assist in the diagnosis of psychiatric disorders.<sup>98</sup> Importantly, CBA approaches are limited by the imperfect correlation between brain function and brain structure.<sup>40, 43</sup> Regarding this, other researchers have proposed the concurrent application of functional activation and connectivity patterns to improve macroanatomical alignment across the whole brain.<sup>99-101</sup> These methods combine curvature-based macroanatomical alignment procedures with an alignment based on functional information in order to further reduce residual interindividual macroanatomical variability. Such variability results from a restricted degree of structural-functional correspondence at some regions due the fact that primarily defined functional loci like V5 and FFA can also vary in size, shape, and anatomical location across subjects.<sup>25, 68, 99-103</sup> An even more complex approach employs “areal features” such as maps of relative myelin content and functional resting state networks to align cortical data.<sup>104</sup> Compared to cortical folding patterns these “areal features” are closer tied to cortical regions thus improving interindividual macroanatomical correspondence to a much larger degree. Nonetheless, to date studies evaluating the potential advantages of these methods for visual field localizer paradigms are lacking.

CBA will be particularly relevant to mitigate the confound of increased macroanatomical variability in neuropsychiatric disorders like SZ to detect true group differences.<sup>44, 105</sup> Such studies are of particular clinical importance since impairments in both the visual system and higher-order cognition are core features of several neuropsychiatric disorders<sup>14, 15, 18, 106-112</sup> including SZ.<sup>5-9</sup> Here, disturbances are described at multiple processing levels<sup>6, 16</sup> including impairments in visual acuity and perceptual organization like deficits in figure-ground segmentation, contour integration, shape completion and detection of coherent motion.<sup>10-15, 17, 18</sup> Several studies imply disturbances in both the ventral and dorsal visual stream to be the cause for the above-mentioned impairments.<sup>17, 18, 113-115</sup> Importantly, these streams show subsequent projections to regions involved in higher-order cognition. Furthermore, neuroplastic alterations in the ventral visual stream have recently been implicated in schizophrenia resilience mechanisms.<sup>116</sup> Importantly, the RDoC project recommends including perceptual and higher-order cognitive processes to establish psychiatric nosology

depending on cognitive dimensions that originate from brain networks rather than from categorical-based classification schemes.<sup>19, 20</sup>

To summarize, our findings provide clear evidence for the superiority of CBA for the study of local visual information processing in early visual areas – particularly at the group-level. Therefore, our paradigm and method are promising to reliably study local information processing in healthy population and its involvement in higher-order cognition including visual selective attention and visual working memory. Also, our paradigm and method can be utilized to reliably study impairments of local visual information processing and disturbances in the interplay between early visual areas and brain regions supporting higher-order cognitive processes in neuropsychiatric disorders. Hence, studying the visual system using reliable methods is of particular importance to increase our understanding of the neurophysiological correlates not only of visual information processing and its interactions with higher-order cognition in health but also of perceptual and cognitive impairments associated with SZ and other neuropsychiatric disorders.

## **Übersicht der Publikation**

Qubad M, Barnes-Scheufler CV, Schaum M, Raspor E, Peters B, Rösler L, Goebel R, Reif A, Bittner RA. Improved correspondence of fMRI visual field localizer data after cortex-based macroanatomical alignment. Scientific Reports. 2022 Aug 22;12:14310



OPEN

# Improved correspondence of fMRI visual field localizer data after cortex-based macroanatomical alignment

Mishal Qubad<sup>1</sup>, Catherine V. Barnes-Scheufler<sup>1</sup>, Michael Schaum<sup>2</sup>, Eva Raspor<sup>1</sup>, Lara Rösler<sup>1,3</sup>, Benjamin Peters<sup>4,5</sup>, Carmen Schiweck<sup>1</sup>, Rainer Goebel<sup>3,6</sup>, Andreas Reif<sup>1</sup> & Robert A. Bittner<sup>1,7✉</sup>

Studying the visual system with fMRI often requires using localizer paradigms to define regions of interest (ROIs). However, the considerable interindividual variability of the cerebral cortex represents a crucial confound for group-level analyses. Cortex-based alignment (CBA) techniques reliably reduce interindividual macroanatomical variability. Yet, their utility has not been assessed for visual field localizer paradigms, which map specific parts of the visual field within retinotopically organized visual areas. We evaluated CBA for an attention-enhanced visual field localizer, mapping homologous parts of each visual quadrant in 50 participants. We compared CBA with volume-based alignment and a surface-based analysis, which did not include macroanatomical alignment. CBA led to the strongest increase in the probability of activation overlap (up to 86%). At the group level, CBA led to the most consistent increase in ROI size while preserving vertical ROI symmetry. Overall, our results indicate that in addition to the increased signal-to-noise ratio of a surface-based analysis, macroanatomical alignment considerably improves statistical power. These findings confirm and extend the utility of CBA for the study of the visual system in the context of group analyses. CBA should be particularly relevant when studying neuropsychiatric disorders with abnormally increased interindividual macroanatomical variability.

The visual system includes a multitude of topographical representations of varying resolution across increasingly specialized visual areas<sup>1</sup>. Functional magnetic resonance imaging (fMRI) offers a variety of methods either to map these topographical representations in full, or to localize specific visual areas or retinotopic positions within their topography. These approaches are essential not only for the fine-grained study of fundamental properties of the visual system<sup>1</sup>, but also for investigating the role of these areas for higher-order cognitive processes such as visual attention and working memory<sup>2–6</sup>. This also extends to translational studies of visual dysfunction and its cognitive consequences in neuropsychiatric disorders<sup>7,8</sup>.

Methods for fMRI-based visual mapping, i.e., techniques to define regions of interest in the visual system based on specific functional properties, fall in in three broad categories: retinotopic mapping, visual field localizer and functional localizer paradigms. Retinotopic mapping and the more advanced population receptive field (pRF) mapping allow the complete delineation of early visual areas<sup>1,9,10</sup>. Conversely, visual field localizer paradigms can map a circumscribed region within a retinotopically organized visual area<sup>11,12</sup>. Finally, functional localizers can detect higher-order visual areas such as the fusiform face area (FFA), parahippocampal place area (PPA), extrastriate body area and lateral occipital complex (LOC), which are clustered and show specialization for the processing of specific categories of complex visual information<sup>1,13,14</sup>. In most fMRI studies, high

<sup>1</sup>Department of Psychiatry, Psychosomatic Medicine and Psychotherapy and Brain Imaging Center, University Hospital Frankfurt, Goethe University, Frankfurt am Main, Germany. <sup>2</sup>Leibniz Institute for Resilience Research, Mainz, Germany. <sup>3</sup>Netherlands Institute for Neuroscience, Amsterdam, The Netherlands. <sup>4</sup>Institute of Medical Psychology, University Hospital Frankfurt, Goethe University, Frankfurt am Main, Germany. <sup>5</sup>Zuckerman Mind Brain Behavior Institute, Columbia University, New York, NY, USA. <sup>6</sup>Department of Cognitive Neuroscience, Faculty of Psychology and Neuroscience, Maastricht University, Maastricht, The Netherlands. <sup>7</sup>Ernst Strüngmann Institute for Neuroscience (ESI) in Cooperation With Max Planck Society, Frankfurt am Main, Germany. <sup>✉</sup>email: robert.bittner@med.uni-frankfurt.de

interindividual anatomical variability of cortical areas in terms of both size and location constitutes an important challenge<sup>15–23</sup>. For instance, it has been shown that primary visual cortex (V1) can differ in size by about twofold between individuals<sup>17</sup>. Furthermore, anatomical variability in terms of location has been shown to be particularly pronounced in extrastriate visual areas<sup>24</sup>. This crucial confound reduces the power to reliably map visual areas at the group level.

One way to mitigate this problem is to pool single-subject regions of interest (ROIs), while simultaneously using the overall group-based probability for that ROI at each point in a Cartesian coordinate system as a constraint<sup>25–27</sup>. While such a single-subject-based analysis improves sensitivity and functional resolution compared to a standard group-based approach, it does not actually reduce macroanatomical variability. Additionally, studying the interplay between visual areas and other cortical areas more directly involved in higher-order cognitive processes with whole-brain methods such as functional connectomics network analyses<sup>28</sup> might preclude a single-subject based strategy.

Group-based analyses typically require spatial normalization of structural and functional imaging data to a common Cartesian coordinate system such as Talairach<sup>29</sup> or MNI<sup>30</sup> space. In its most basic form, volume-based spatial normalization employs a linear transformation that matches the overall extent of the brains to a standard brain template. While transformation into Talairach space relies on anatomical landmarks, transformation into MNI space utilizes fully data-driven registration of structural images to an average template brain<sup>30</sup>. While these spatial normalization approaches inherently result in an alignment of brains, the underlying algorithms are not optimized specifically for aligning homologous brain structures. Conversely, more refined methods employ non-linear warping algorithms guided by intensity differences to improve macroanatomical alignment<sup>31</sup>. Thus, all of these methods can be categorized as volume-based alignment (VBA) techniques. However, both linear and nonlinear VBA mostly disregard the topological properties of the cerebral cortex and its geometric features such as sulci and gyri. Consequently, VBA methods result in a considerable amount of residual interindividual anatomical variability<sup>32,33</sup>.

Surface-based procedures constitute an important alternative approach. Surface-based spatial normalization typically uses a geodesic coordinate system, which allows for a two-dimensional representation of the cerebral cortex and respects the cortical topography to a much larger degree than traditional Cartesian coordinate systems<sup>18,34</sup>. This approach offers two main advantages over VBA. First, surface-based spatial normalization allows to constrain data readout and data pre-processing such as spatial smoothing to cortical tissue. This reduces signal contamination by white matter and cerebrospinal fluid substantially and also mostly precludes contamination from cortical areas proximal in volume space but considerably more distant in surface space. Overall, this approach enhances the signal-to-noise ratio (SNR). Consequently, spatial smoothing in surface space is superior to spatial smoothing in volume space<sup>19,35</sup>. The second advantage of surface-based spatial normalization is the possibility to use individual cortical folding patterns for an additional, fully data-driven macroanatomical alignment of the cerebral cortex<sup>34</sup>. Compared to VBA techniques, these cortex-based alignment (CBA) methods considerably improve anatomical correspondence of cortical structures while respecting cytoarchitectonic boundaries<sup>36</sup>. Thus, CBA leads to a notable reduction of interindividual anatomical variability<sup>18,34,37–39</sup>.

Importantly, previous studies have often exclusively compared surface-based data before and after macroanatomical alignment<sup>19,40</sup>, essentially using the former approach as a proxy for VBA. Yet, this comparison only reflects the second advantage of CBA, namely the use of macroanatomical alignment instead of VBA. However, in this case both data sets benefit equally from reduced signal contamination, likely underestimating the full effects of CBA. Assessing the impact of this first advantage of surface-based analyses in isolation requires a comparison of VBA with a surface-based analysis without macroanatomical alignment. We refer to this intermediate approach as a “surface-based analysis using VBA” (SBAV). Thus, assessing both benefits of CBA requires the comparison of three approaches: VBA, SBAV and CBA.

Due to the advantageous properties outlined above, CBA methods have been proposed as an alternative approach to VBA specifically for the visual system<sup>26</sup>. Several studies have compared the impact of VBA and CBA methods on specific visual mapping techniques. For retinotopic mapping, an improvement of functional overlap in both V1 and V2 after CBA has been demonstrated<sup>34,41</sup>. For functional localizer data, CBA substantially increases the overlap of object processing areas LOC, FFA and PPA across subjects<sup>19,42–44</sup>. Conversely, the effects of CBA on visual field localizer paradigms mapping specific retinotopic positions have not been studied. Thus, the utility of CBA has been demonstrated for two of the three main categories of visual mapping methods, i.e., those methods, which map whole areas, either defined primarily by cytoarchitectonic (e.g. V1) or functional (e.g. FFA) properties. Conversely, it remains unclear, to which degree CBA can improve the alignment of ROIs mapped by visual field localizer paradigms. Such paradigms are required for the detailed study of the local processing of simple visual stimuli in early visual areas<sup>11,12,45–47</sup>. Flashing checkerboards covering the exact area of interest within the visual field are primarily used for this purpose. Checkerboards lead to a particularly strong BOLD-signal increase in early visual areas (V1–V3)<sup>48</sup>. To maximize fidelity of the resulting localizer maps, visual field localizer paradigms typically utilize the fact that attentional modulation induced by task demands significantly enhances response reliability across visual areas. This can be achieved by adding a simple target-detection task<sup>49</sup>.

We used such an attention-enhanced visual field localizer paradigm to map a circumscribed location in each visual quadrant across early visual areas aiming to define ROIs suitable for the study of higher cognitive processes. We chose a CBA method using a dynamic group average as the target brain<sup>19</sup>. Thus, we eliminated the possible confound of a static CBA target based on an individual brain, whose cortical folding pattern might by chance deviate considerably from the group average.

Our primary goal was to examine the effects of CBA for a visual field localizer paradigm. More specifically, we aimed to determine, whether macroanatomical alignment improves the reliability of mapping subregions within retinotopically organized visual areas delineated by such a paradigm at the group level. To this end, in addition to the analysis of the full single-subject ROIs, we also examined the correspondence of single-subject ROI peak

vertices, i.e., single vertices showing the strongest level of activation in each subject for each visual quadrant. We conducted this analysis, because peak vertices are a good approximation of the center of a ROI and thus allow for a more precise assessment and visualization of the effects of macroanatomical alignment. Based on previous findings for other localizer paradigm classes and the relatively good structural–functional correspondence in posterior occipital cortex, we expected to observe a benefit of CBA compared to SBAV when aligning subregions within early visual cortex for both full ROIs and peak vertices.

Our second goal was to examine the effects of SBAV. More specifically, we aimed to assess the impact of surface-based functional data readout and pre-processing without macroanatomical alignment. Here, we expected a general improvement of the SNR for SBAV compared to VBA and a corresponding global increase in group ROI size for all visual quadrants. Notably, several studies have shown differential response properties such as receptive field size by visual quadrant or hemifield for homologous early visual areas. For instance, previous studies reported improved behavioral performance and higher BOLD-signal amplitudes in the lower visual hemifield<sup>50–53</sup>. We were therefore also interested, whether we could observe differences between upper and lower visual hemifields in our group analysis after CBA.

Overall, the aim of the study was to close an important gap in the evaluation of CBA for the study of the visual system. Since visual field localizers are crucial for investigating contributions of the visual system to higher-order cognitive processes, our results should have implications for the study of visual cognition in both basic and translational neuroscience research.

## Results

**Visual quadrant ROIs (group level).** Group-level mapping of the four visual quadrants revealed notable differences for the three alignment techniques (VBA, SBAV, CBA) (Fig. 1, Tables 1, 2). For the lower right visual quadrant, ROI size increased considerably from VBA to SBAV, but decreased for CBA (Table 2). For the lower left visual quadrant, ROI size decreased slightly from VBA to SBAV, but increased considerably for CBA. For the upper left visual quadrant, ROI size increased considerably from VBA to SBAV and increased further for CBA. For the upper right visual quadrant, ROI size increased slightly from VBA to SBAV and increased considerably for CBA. Thus, two out of four visual quadrant ROIs exhibited a pattern of continuously increasing cluster size, reflecting an expansion of significant position selectivity across alignment techniques. Additionally, while ROI size for the lower left visual quadrant decreased slightly from VBA to SBAV, ROI size for CBA was also by far the largest. Furthermore, while ROI size decreased for the lower right visual quadrant after CBA, for SBAV this ROI showed by far the greatest extent of any ROI for any alignment technique, even encompassing posterior parts of temporal cortex.

Within group ROIs, average time courses showed clear position selectivity, which was not further affected by alignment technique as indicated by the negative results of our linear mixed models (Table 3). Notably, asymmetry indices (AIs) revealed markedly greater vertical symmetry of both upper and lower hemifield ROIs for VBA and CBA compared to SBAV (Table 4). After CBA, ROI sizes for the lower visual hemifield were considerably larger than for the upper visual hemifield (Table 1).

**Probability maps.** For all three data sets, the maximum probability of activation overlap was consistently located at the center of each ROI as defined in our previous group analysis (Fig. 1, Tables 1, 5). For VBA data, probability maps (PMs) showed a relatively wide spread of functional activation around the core ROIs (Fig. 2a, Table 5). Maximum probability of activation overlap was 55%. For SBAV data, PMs showed an even wider spread of functional activation around the core ROIs (Fig. 2b, Table 5). Maximum probability of activation overlap was 66%. For CBA data, PMs showed a noticeable decrease in the spread of functional activation around the core ROIs with a corresponding increase in the maximum probability of overlap at the center of the core ROIs (Fig. 2c, Table 5). Maximum probability of activation overlap was 86%.

**Probability difference maps.** Probability difference maps (PDMs) revealed a differential impact of the individual methodological elements of our macroanatomical alignment approach.

For pure surface-based functional data readout and pre-processing compared to standard volume-based alignment, the corresponding PDM (SBAV minus VBA) showed a maximum increase in the probability of activation overlap of 30% around the central ROIs. Conversely, at the location corresponding to the central group ROIs we mostly observed a decrease in the probability of activation overlap of up to 19% (Fig. 3a, Table 6). Notably, changes were widespread, partly extending into posterior temporal and parietal cortex. For the addition of macroanatomical alignment, the corresponding PDM (CBA minus SBAV) showed a maximum increase in the probability of activation overlap of 44% in the central ROIs (Fig. 3b, Table 6). Conversely, more peripheral occipital regions showed a maximum decrease in the probability of activation overlap of 32%. Overall, changes were considerably less widespread than for the SBAV minus VBA comparison. For the additive impact of both methodological elements, the corresponding PDM (CBA minus VBA) showed a maximum increase in the probability of activation overlap of 52% in the central ROIs (Fig. 3c, Table 6). Conversely, more peripheral occipital regions as well as posterior temporal and parietal cortex showed a maximum decrease in the probability of activation overlap of 36%. Overall, the spatial extent of these effects fell in between that of the other two comparisons.

**Spatial variability of ROI peak vertex distribution (single-subject level).** The rates of success for detecting subject–subject ROIs were as follows: lower right visual quadrant 98% (49 out of 50 subjects), lower left visual quadrant 94% (47 out of 50 subjects), upper left visual quadrant 98% (49 out of 50 subjects), upper right visual quadrant 90% (45 out of 50 subjects). Mirroring group-level PMs, single-subject level peak vertex distribution maps (Fig. 4) showed reduced spatial variability for CBA compared to SBAV. Furthermore, for CBA

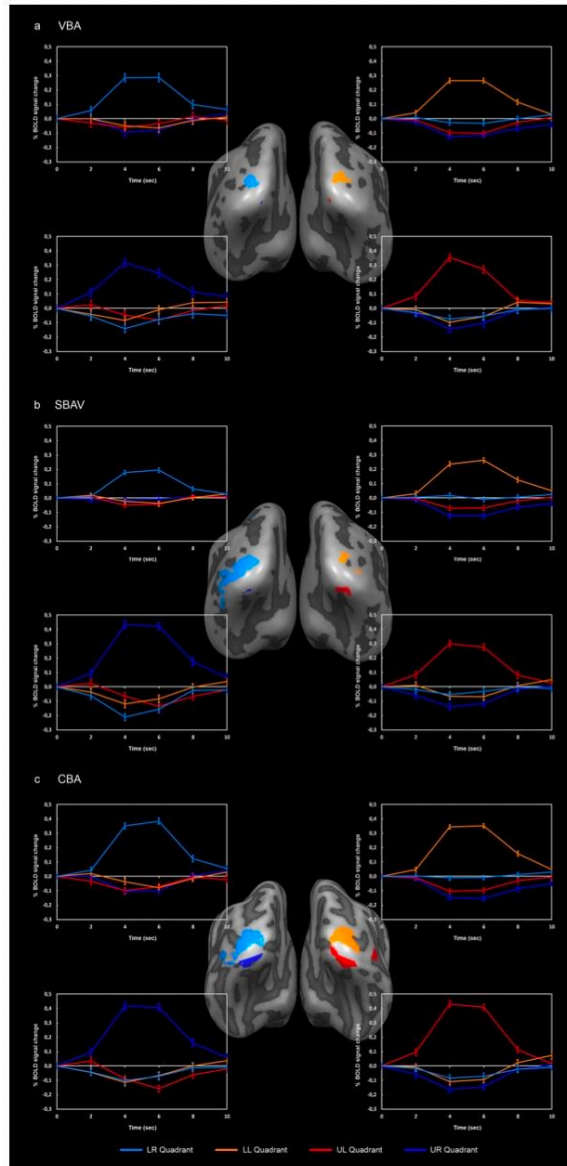


**Figure 1.** Group analysis of visual quadrants. (a) VBA results. Maps and average timecourses were computed in volume space; maps were projected on the non-aligned average surface representation. (b) SBAV results. Maps and average timecourses were computed in surface space; maps were projected on the non-aligned surface representation. (c) CBA results. Maps and average timecourses were computed in surface space; maps were projected on the aligned average surface representation. Overall, two out of four visual quadrant ROIs exhibited a pattern of continuously increasing cluster size, reflecting an increasing extent of significant position selectivity across alignment techniques. Additionally, while ROI size for the lower left visual quadrant decreased slightly from VBA to SBAV, ROI size for CBA was also by far the largest. Only the ROI of the lower right visual quadrant showed a cluster size decrease after CBA. Average timecourses (incl. standard error of the mean) showed clear position selectivity with a strong BOLD signal increase for the position of interest and no BOLD signal increase for the other three positions. ROI/graph colors: light-blue = lower right (LR) visual quadrant, orange = lower left (LL) visual quadrant, red = upper left (UL) visual quadrant, dark-blue = upper right (UR) visual quadrant.



Region of interest	Analysis method	Number of vertices	Number of voxels	TAL coordinates		
				x	y	z
Lower right visual quadrant	VBA	47	953	-22	-90	2
	SBAV	295	NA	-42	-64	5
	CBA	161	NA	-24	-91	-4
Lower left visual quadrant	VBA	46	828	19	-94	2
	SBAV	28	NA	23	-90	3
	CBA	127	NA	9	-94	-5
Upper left visual quadrant	VBA	4	55	4	-87	-9
	SBAV	47	NA	24	-75	-14
	CBA	82	NA	18	-77	-15
Upper right visual quadrant	VBA	3	1	-5	-88	-13
	SBAV	6	NA	-18	-80	-15
	CBA	58	NA	-18	-80	-15

**Table 1.** Group ROIs. Size and Talairach coordinates of the group ROIs of the corresponding visual quadrants for the VBA, SBAV and CBA data sets. For ROI size comparison, we focused exclusively on the number of vertices. Importantly, we only provide the number of voxels of each VBA ROI as a reference to ensure a comprehensive reporting of our findings. In three out of four visual quadrant ROIs we observed the largest cluster size for CBA, which is indicative of the highest degree of position selectivity for the most advanced alignment technique.

	VBA → SBAV (%)	VBA → CBA (%)	SBAV → CBA (%)
Lower right visual quadrant	528	243	-45
Lower left visual quadrant	-39	176	354
Upper left visual quadrant	1075	1950	74
Upper right visual quadrant	100	833	867

**Table 2.** Changes of group ROI size compared between alignment methods. We used the following formula:  $\frac{\text{size\_ROI}_{Quad}[AM_n] - \text{size\_ROI}_{Quad}[AM_m]}{\text{size\_ROI}_{Quad}[AM_n]} \times 100$ . For SBAV compared to VBA, we observed a group ROI size increase in three out of four visual quadrants. For CBA compared to VBA, we observed a group ROI size increase in all four visual quadrants. For CBA compared to SBAV we observed a group ROI size increase in three out of four visual quadrants. *Quad* visual quadrant of interest, *AM* alignment method (VBA, SBAV, CBA). *n* and *m* specify AMs, with *m* referring to the less advanced AM and *n* referring to the comparatively more advanced AM.

visual quadrant	Sum Sq	Mean Sq	NumDf	DenDf	F value	p value	p value (corr.)
Lower right visual quadrant	183.2	92	2	147*	0.31	0.737	1.000
Lower left visual quadrant	2660.2	1330.1	2	98	1.25	0.291	1.000
Upper right visual quadrant	2546.2	1273.1	2	98	3.36	0.039	0.156
Upper left visual quadrant	73678	36839	2	98	1.19	0.308	1.000

**Table 3.** Effect of alignment method on position selectivity within group ROIs. To test whether the strength of position selectivity within corresponding group ROIs across alignment techniques increases for the more advanced alignment techniques, we conducted separate linear mixed models with random intercept for each visual quadrant. For each position, we used each subject's t-values as the dependent variable and the alignment techniques (VBA, SBAV and CBA) as the independent variable. We adjusted p-values using Bonferroni correction. We did not observe any significant effect (all *p* adjusted > 0.05), indicating that this measure of position selectivity within corresponding group ROIs was not affected by alignment technique. Thus, while for each alignment method and visual quadrant the corresponding ROI did show significant position selectivity, the strength of within-ROI position selectivity did not increase for more advanced alignment techniques. \*Random effect variance estimate at the subject-level for the LR ROI was 0, resulting in a singular fit when using lmer. Therefore, results for LR were estimated without random intercept are thus equivalent to a regular ANOVA. *Sum Sq* sum of squares, *Mean Sq* mean square, *NumDf* degrees of freedom in the numerator, *DenDf* degrees of freedom in the denominator.

Symmetry	ROI comparison	AI (VBA)	AI (SBAV)	AI (CBA)
Vertical	LR and LL	1.1	82.7	11.8
	UL and UR	14.3	77.4	17.1
Horizontal	LR and UR	88.0	96.0	47.0
	LL and UL	84.0	25.3	21.5

**Table 4.** Vertical and horizontal asymmetry indices (AIs). To assess the impact of the three alignment techniques on horizontal and vertical symmetry of our group-level ROIs, we computed a ROI size AI between each pair of ROIs. AIs revealed greater vertical symmetry of the upper and lower hemifield ROIs for VBA and CBA compared to SBAV. *LR* lower right visual quadrant, *LL* lower left visual quadrant, *UL* upper left visual quadrant, *UR* upper right visual quadrant.

Probability map	Analysis method	Number of vertices	MPO (%)	TAL		
				x	y	z
Lower right visual quadrant	VBA	1243	55	-22	-89	-2
	SBAV	2074	66	-26	-87	2
	CBA	1391	86	-20	-93	-1
Lower left visual quadrant	VBA	853	53	23	-89	1
	SBAV	1396	56	20	-93	0
	CBA	918	84	20	-93	1
Upper left visual quadrant	VBA	958	50	15	-84	-13
	SBAV	1401	60	13	-78	-16
	CBA	1162	80	18	-83	-12
Upper right visual quadrant	VBA	965	47	-19	-81	-14
	SBAV	1897	48	-14	-83	-14
	CBA	1445	76	-15	-87	-15

**Table 5.** Extent of probability maps. For each visual quadrant and analysis methods, we counted the number of vertices in the corresponding probability maps exceeding the threshold of 10% probability of activation overlap. For VBA, maximum probability of activation overlap (MPO) was 55%. For SBAV, maximum probability of activation overlap was 66%. For CBA, maximum probability of activation overlap was 86%. We also extracted the Talairach (TAL) coordinates of the vertex showing MPO for each quadrant and each data set.

compared to SBAV we observed an increase in the number of multiple overlapping single-subject ROI peak vertices per vertex for each visual quadrant (Table 7).

## Discussion

The aim of our study was to evaluate the utility of CBA for an attention-enhanced visual field localizer paradigm used to map circumscribed regions within retinotopically organized visual areas. Our paradigm mapped homologous regions in each visual quadrant reliably across early visual areas. As expected, CBA led to a marked reduction in macroanatomical variability with a number of beneficial effects on the functional level, which clearly exceeded those observed for SBAV. Compared to VBA and SBAV, CBA resulted in the most consistent improvements in the group ROI analysis across visual quadrants (Fig. 1).

For SBAV compared to VBA, we observed a group ROI size increase in three out of four visual quadrants (Fig. 1, Tables 1, 2). For CBA compared to VBA, we observed a group ROI size increase in all four visual quadrants. For CBA compared to SBAV we observed a group ROI size increase in three out of four visual quadrants.

These results indicate an improved power for CBA to detect subregions of early visual areas, which show position selectivity. Conversely, we did not observe an increase of position selectivity within corresponding visual quadrant ROIs across alignment techniques in our linear mixed model analysis (Table 3). However, CBA was the only approach leading to both an increase in ROI size and a preservation not only of vertical but also of horizontal symmetry (Table 4).

Regarding changes in the probability of activation overlap across the three alignment techniques reflected by the PMs, a clear pattern emerged. Probability of activation overlap increased gradually with each step, peaking for CBA with a maximum value of 86%. For SBAV, effects were weaker and considerably more widespread, mostly affecting more peripheral brain regions. Likewise, for the comparison of CBA and SBAV PDMs showed an increase in the probability of activation overlap with a maximum of 44% at the central locations corresponding to the group ROIs. This resulted in considerably more focused activation patterns, while the opposite effect emerged at more peripheral vertices (Fig. 3). This is most likely not attributable to a decreased spatial overlap in the periphery of early visual areas. Rather, it indicates that CBA consistently reduces spurious spread-out activation resulting from poor macroanatomical correspondence after VBA and a generalized SNR increase due

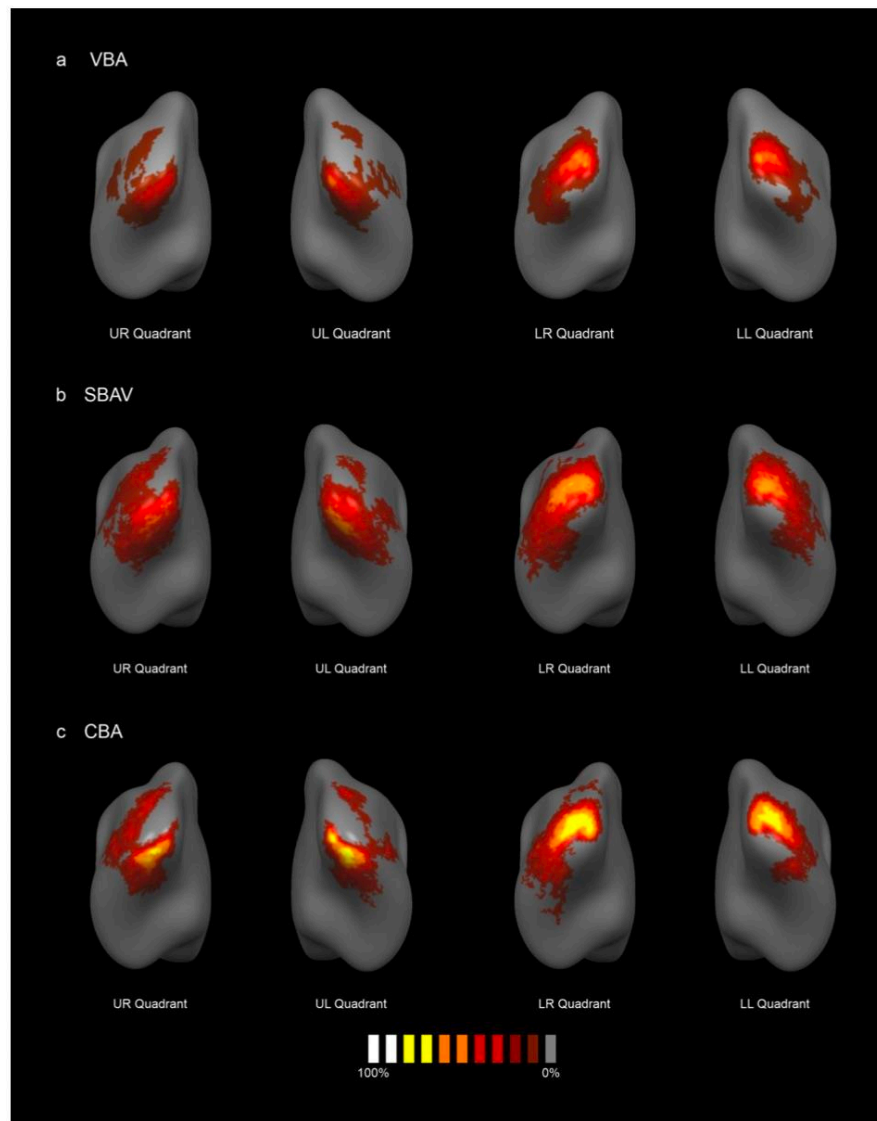


**Figure 2.** Probability maps (PMs). PMs indicating the probability of activation overlap across subjects for each visual quadrant. The color code gray-to-white indicates the probability of activation overlap of single-subject maps, thresholded at a minimum of 10% probability of activation overlap. Single-subject maps were thresholded at  $p < 0.05$  (uncorr.). We also applied a cluster level threshold of 100 vertices. (a) PMs for VBA showed a maximum probability of activation overlap of up to 55%. (b) PMs for SBAV showed a maximum probability of activation overlap of up to 66%. (c) PMs for CBA showed a maximum probability of activation overlap of up to 86%.

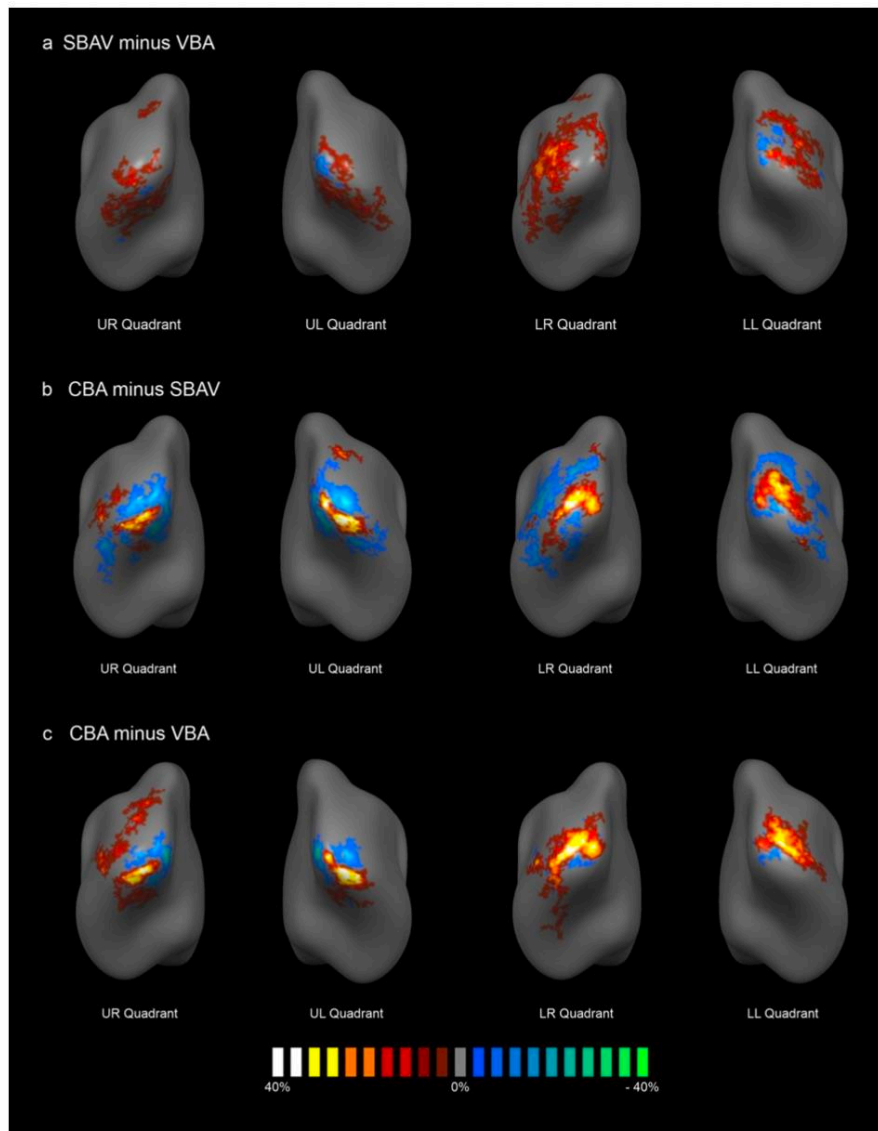


**Figure 3.** Probability Difference Maps (PDMs). PDMs indicating the differential impact of the individual steps of our overall macroanatomical alignment approach for each visual quadrant. PDMs were generated using PMs derived from single-subject maps. PMs were unthresholded. The color code indicates the difference of activation overlap. The color code brown-to-white indicates a higher degree of functional activation overlap for the more advanced alignment method. The color code blue-to-green indicates a higher degree of functional activation overlap for the less advanced alignment method. PDMs were thresholded at a minimum probability difference of 5%. (a) The impact of surface-based functional data readout and pre-processing compared to standard volume-based alignment (SBAV minus VBA) was characterized by a widespread activation with an increase in the probability of activation overlap of up to 30% around the central ROIs and a decrease in the probability of activation overlap of up to 19% at the location corresponding to the central ROIs. (b) The additional impact of macroanatomical alignment (CBA minus SBAV) was less widespread but characterized by an increase in the probability of activation overlap of up to 44% at the location of the central ROIs and a decrease in the probability of activation overlap of up to 32% around the central ROIs. (c) The additive impact of both methodological elements (CBA minus VBA) was characterized by an increase in the probability of activation overlap of up to 52% at the location of the central ROIs and a decrease in the probability of activation overlap of up to 36% around the central ROIs.

Probability difference map	Analysis method	Number of vertices	PD pos (%)	PD neg (%)	TAL PD pos			TAL PD neg		
					x	y	z	x	y	z
Lower right visual quadrant	SBAV minus VBA	1169	30	-12	-34	-76	4	-16	-98	-3
	CBA minus SBAV	1341	40	-28	-24	-90	-3	-42	-75	6
	CBA minus VBA	739	46	-15	-25	-88	-3	-24	-84	9
Lower left visual quadrant	SBAV minus VBA	570	23	-16	33	-80	5	20	-92	10
	CBA minus SBAV	694	38	-22	22	-91	5	27	-77	11
	CBA minus VBA	402	43	-16	22	-92	-2	18	-96	-8
Upper left visual quadrant	SBAV minus VBA	612	25	-19	18	-72	-14	12	-89	-5
	CBA minus SBAV	680	44	-32	17	-82	-12	10	-76	-15
	CBA minus VBA	546	52	-36	18	-83	-12	11	-86	-4
Upper right visual quadrant	SBAV minus VBA	689	25	-13	-19	-69	-9	-9	-86	-7
	CBA minus SBAV	964	36	-32	-15	-87	-15	-15	-72	-12
	CBA minus VBA	795	43	-34	-15	-87	-15	-7	-84	-6

**Table 6.** Extent of probability difference maps (PDMs) including positive and negative foci. For each visual quadrant and comparison between analysis methods (SBAV minus VBA, CBA minus SBAV, CBA minus VBA), we counted the number of vertices in the corresponding PDMs exceeding the threshold of plus 5% or minus 5% difference in probability of activation overlap. Overall, the extent of PDMs was greatest for the CBA minus VBA comparison, i.e., the combined effect of surface-based analysis and macroanatomical alignment. We also extracted Talairach (TAL) coordinates of the positive and negative foci for each quadrant and each data set. *PD pos* positive value of probability difference, *PD neg* negative value of probability difference.

to SBAV. It also suggests that VBA and SBAV might misrepresent the location and extent of early visual areas. This notion is supported by changes of the center of gravity of group ROIs between SBAV and CBA, which were particularly pronounced for the lower left visual quadrant (Table 1). Together, these findings indicate that CBA substantially increases statistical power when studying early visual areas at the group level. Naturally, this effect of CBA should also extend to studies with a more global focus, such as connectivity analyses<sup>35,54</sup>.

Additionally, the specific advantages of CBA were evident in the markedly decreased variability of single-subject ROI peak vertex locations for each visual quadrant compared to SBAV (Fig. 4, Table 7). This is indicative of a reduction of macroanatomical and functional inter-subject variability achieved by CBA as the main reason for the improved group-level results. Our findings confirm that transforming functional data from volume-space into surface space already increases statistical power by reducing signal contamination from non-neuronal tissue, thus improving the SNR. Consequently, using SBAV as a proxy for VBA would underestimate the actual benefits of CBA. Our findings indicate that only the CBA approach benefits from both an improved SNR and reduced macroanatomical variability. Thus, our data support the notion that among evaluated methods, CBA is the most advantageous alignment technique for studying the visual system. Such an interpretation is also supported by the fact that only CBA but not SBAV could preserve the vertical symmetry of group ROIs characteristic of early visual areas, which was already evident for VBA (Table 4). This discrepancy is most likely attributable to the unspecific SNR increase induced by SBAV, which in combination with its inherently poor macroanatomical alignment does not result in a consistent improvement of functional overlap for all visual quadrants.

For VBA, we observed the largest group ROIs for the right and left lower visual quadrants, an effect that changed after SBAV and CBA (Fig. 1a, Table 1). For SBAV, we observed the largest group ROIs for the left upper and right lower visual quadrants, which did not persist after CBA (Fig. 1b,c, Table 1). Notably, several studies reported lateralized effects on neurophysiological parameters in early visual areas<sup>55,56</sup>. Our observation raises the question, whether these findings could at least partly be explained by lateralized differences in macro-anatomical variability rather than true functional differences.

Conversely, our CBA-aided group analysis allowed us to compare the response properties of each visual quadrant in a more unbiased way. We observed larger group ROIs for the lower visual hemifield. In a CBA-based probabilistic atlas of the visual system, which included all regions that could be defined in more than 50% of subjects, probabilistic ROIs for dorsal V1 and V2 were also noticeably larger than probabilistic ROIs for ventral V1 and V2, whereas this effect was less clear for V3<sup>45</sup>. These results are in line with our own findings and could be attributable to higher residual anatomical variability after CBA in ventral occipital cortex representing the upper visual hemifield. Alternatively, they could be due to true differences in response properties such as receptive field size or overall area size. The latter interpretation is supported by studies showing functional differences between upper and lower visual hemifields already at the retinal level in the form of differences in receptor densities<sup>57,58</sup>. Cone density was higher in the superior parts of the retina, which processes information from lower visual fields. Conversely, higher rod density was observed in the inferior parts. Moreover, Eickhoff et al. reported dorso-ventral asymmetries in receptor densities in V2 and V3<sup>37</sup> and higher GABA-A and muscarinic M3-receptor density in ventral parts of V2 and V3. Furthermore, there is evidence for fundamental differences in receptive field shape from pRF mapping<sup>59</sup>. Estimating both the aspect ratios and the size of mapped areas, a more elliptical receptive field shape was observed for the upper visual hemifield represented by ventral parts of the visual cortex compared to the lower visual hemifield represented by dorsal parts of the visual cortex. Additionally, there is evidence for a behavioral advantage in the lower visual hemifield for shape discrimination as well as higher BOLD-signal

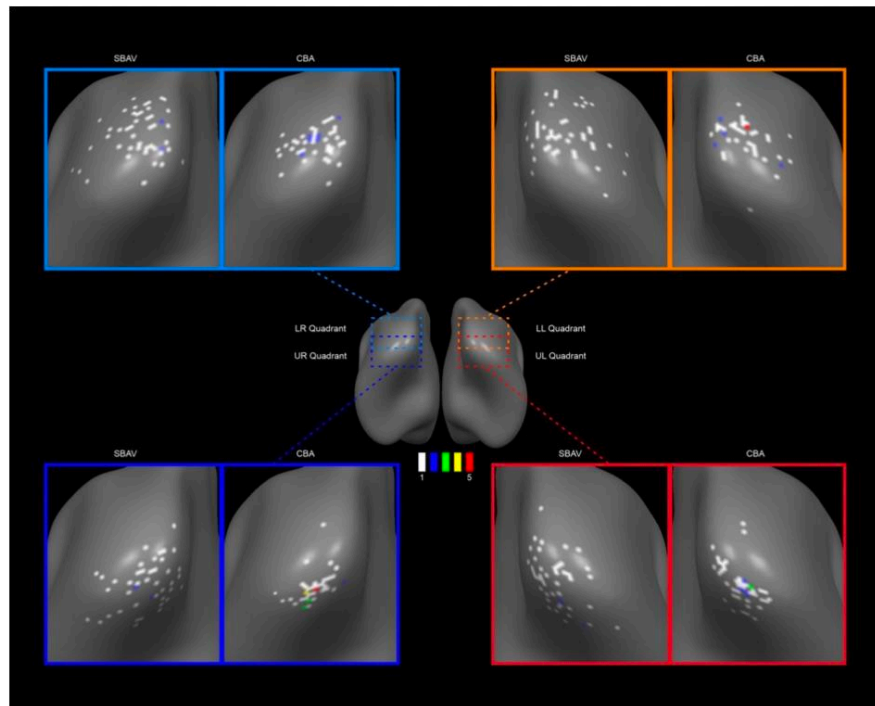


**Figure 4.** Single-subject peak vertex distribution maps for SBAV and CBA data sets. We mapped single-subject peak vertices for each visual quadrant in surface space for SBAV and CBA data. We then calculated the vertex-wise number of single-subject peak vertices. The color code indicates the number of overlapping single-subject ROI peak vertices per vertex. We observed an increase in the number of overlapping single-subject ROI peak vertices per vertex after macroanatomical alignment (CBA). The number of single-subject peak vertices per occipital vertex for each visual quadrant before and after macroanatomical alignment (SBAV and CBA) ranged between 1 and 5. Thus, a higher number indicates an improved alignment precision of single-subject ROI peak vertices. *LR* lower right visual quadrant, *LL* lower left visual quadrant, *UL* upper left visual quadrant, *UR* upper right visual quadrant.

changes and peak amplitudes of MEG/EEG responses<sup>50,52,53,60,61</sup>. Together, these findings demonstrate clear differences in the functional architecture of early visual areas representing the upper and lower visual hemifield, respectively. This has been attributed to the fact that the lower visual hemifield represented by dorsal parts of the occipital lobe is more closely linked to the dorsal visual pathway, while the upper visual hemifield represented by ventral parts of the occipital lobe is more closely linked to the ventral visual pathway<sup>62,63</sup>. Furthermore, there is evidence for fundamental differences in receptive field shape from pRF mapping<sup>59</sup>. Here, for the upper visual hemifield represented by ventral parts of the visual cortex, an increased size and more elliptical shape of receptive fields was observed compared to the lower visual hemifield represented by dorsal parts of the visual cortex. This implies that the lower visual field is more specialized for the precise localization and representation of space. Our observation of larger ROIs in the lower visual hemifield is in line with these findings. Hence, our results imply that CBA is a suitable tool to extend the study of functional and behavioral asymmetries in early visual areas to the group-level.

One important limitation of the current study is the lack of complementary retinotopic mapping data due to time constraints. This data would have allowed us to delineate the boundaries of early visual areas and pinpoint the exact visual area containing each individual single-subject ROI. Retinotopic mapping studies indicate that peak activation of single subjects elicited by visual localizers are not consistently located in the same visual area. Most localizer paradigms show peak activation not in V1 but rather in V2 or V3<sup>12</sup>. It is therefore highly likely that our single-subject peak activation did not consistently belong to the same visual cortical area. With the current data set we cannot determine how precisely individual visual areas were aligned with CBA, and whether individual levels of the visual cortical hierarchy were affected differentially. However, the position of our group ROIs, which bordered the calcarine sulcus and spanned the occipital pole, indicate that they mainly comprised V2 and V3. Similarly, after CBA we observed a comparable increase in the probability of overlap in the same part

# of PV per vertex	LR		LL		UL		UR		Overall	
	SBAV	CBA	SBAV	CBA	SBAV	CBA	SBAV	CBA	SBAV	CBA
1 (no overlapping PV)	45	37	47	34	43	38	41	28	176	137
2 overlapping PV	2	6	0	4	3	4	2	1	7	15
3 overlapping PV	0	0	0	0	0	1	0	2	0	3
4 overlapping PV	0	0	0	0	0	0	0	1	0	1
5 overlapping PV	0	0	0	1	0	0	0	1	0	2
PV detection success rate (%)	98		94		98		90		95	

**Table 7.** Single-subject ROI peak vertex distribution maps. We mapped all single-subject ROI peak vertices per visual quadrant for SBAV and CBA. We quantified alignment precision of these peak vertices by counting for each occipital vertex the number of overlapping peak vertices for SBAV and CBA. The number of single-subject peak vertices per occipital vertex for each visual quadrant before and after macroanatomical alignment (SBAV and CBA) ranged between 1 and 5. Thus, a higher number indicates improved alignment precision of single-subject ROI peak vertices. After CBA, we observed an increase in the number of multiple, i.e. overlapping, single-subject ROI peak vertices per occipital vertex for each visual quadrant and a corresponding decrease in the number of non-overlapping single-subject ROI peak vertices per occipital vertex. The last row contains the success rate of detecting single-subject ROIs and ergo peak vertices for each visual quadrant. Success rates are necessarily equal for SBAV and CBA, because this aspect of our single-subject analysis cannot be influenced by alignment method. *PV* single-subject ROI peak vertex, *LR* lower right visual quadrant, *LL* lower left visual quadrant, *UL* upper left visual quadrant, *UR* upper right visual quadrant.

of occipital cortex. While this is at least suggestive of a relatively consistent benefit of CBA across visual areas, more fine-grained studies including retinotopic mapping are required to address this issue more definitively.

Furthermore, we did not use eye tracking to ensure sufficient fixation. We also did not include an additional attentional control task centered on the fixation cross, which would have further encouraged continuous fixation. This omission was deliberate in order to keep the difficulty level adequate for psychiatric patient populations. Our average success rate for finding reliable activation in early visual areas across all four visual quadrants was 95 (90–98)%. Insufficient fixation might partly explain our failure to find reliable activation in a small fraction of subjects.

Finally, several properties of the VBA data set differed from the SBAV and CBA data sets. We could not match volume-based and surface-based pre-processing parameters completely due to inherent differences between the three-dimensional and two-dimensional spatial smoothing algorithms employed. Importantly, the number of voxels and vertices containing functional data were not identical, differentially affecting Bonferroni correction of group results. The smaller analysis space of the VBA data set—69% the size of the SBAV and CBA data set—lead to a corresponding less strict Bonferroni-corrected, final statistical threshold for VBA. Due to this bias towards the VBA data set, the beneficial effects of the additional processing steps featured in the SBAV and CBA data sets should be underestimated. The fact that we could demonstrate the advantages of CBA despite an unfavorable statistical threshold for confirming this primary hypothesis underscores the superiority of this alignment technique.

Our study also has implications beyond mapping the visual system in healthy populations. Visual processing deficits are a prominent feature of neurodevelopmental psychiatric disorders such as ADHD, schizophrenia and autism spectrum disorders<sup>7,8,64–71</sup>, which can also perturb crucial higher-order cognitive processes including working memory<sup>72–74</sup>. The current localizer paradigm will be useful to investigate local impairments of visual information processing as well as disturbances in the interplay between early visual areas and brain networks supporting higher-order cognitive processes. Here, CBA will be particularly relevant to reduce the confounding effects of increased macroanatomical variability in disorders such as schizophrenia in order to measure true group differences and true functional variability<sup>37,75</sup>. On the other hand, CBA might also be crucial for investigating the neurodevelopmental underpinnings of increased macroanatomical variability itself. To this end, the inclusion of probabilistic atlases containing information about gene expression profiles<sup>76</sup> as well as cyto- and receptor architectonics<sup>77,78</sup> will be valuable.

Our CBA approach relied solely on cortical curvature information to reduce macroanatomical variability. One main advantage of this method is its feasibility for the vast majority of fMRI data sets, since it only requires a structural brain scan of sufficient quality and resolution. Among comparable methods, CBA is the most data-driven and objective approach. However, the achievable reduction of macroanatomical variability is limited by the variable and imperfect correlation between brain structure and brain function<sup>34,39</sup>. Consequently, more advanced methods additionally utilize orthogonal functional data to further reduce anatomical variability, including the use of functional activation or connectivity patterns to improve macroanatomical alignment across the whole brain<sup>20,79,80</sup>. Additionally, a more complex approach has been proposed, which aligns cortical data using ‘areal features’ more closely tied to cortical areas than cortical folding patterns, including maps of relative myelin content and functional resting state networks<sup>81</sup>. These methods have shown to provide a relevant additional reduction of macroanatomical variability for a variety of paradigms including visual functional localizers. Future studies should also evaluate these methods for retinotopic mapping and visual field localizers. Moreover, it has been demonstrated for early auditory areas, that the additional use of a probabilistic atlas of cytoarchitectonically defined areas further enhances standard CBA results<sup>82</sup>. In principle, such an approach should easily be feasible for the visual system.

To summarize, we demonstrated clear advantages of CBA compared to VBA for the analysis of visual field localizer data at the group-level, signified by a considerable reduction of spatial variability across subjects across early visual areas. Our findings extend previous CBA studies evaluating other major categories of visual mapping techniques. They underscore the loss of information and statistical power incurred by the use of VBA methods in the majority of fMRI studies. Therefore, CBA and comparable methods should be seriously considered as a standard procedure for the detailed study of visual information processing and its disturbance in neuropsychiatric disorders.

## Methods and materials

**Participants.** All participants gave their written informed consent to participate in the study in accordance with the study protocol approved by the ethical review board of the Faculty of Medicine at Goethe University. We conducted all experimental procedures in conformity with the approved guidelines and the Declaration of Helsinki. Individuals received compensation for their participation. We recruited 51 healthy volunteers (female:male = 28:23) with age ranging between 18 and 43 years (mean = 24). All participants were non-smokers, had no history of neurological or psychiatric illness and reported normal or corrected-to-normal visual acuity. One participant was left-handed as assessed by the German version of the Edinburgh Handedness Inventory<sup>83</sup>.

**Stimuli and task.** Subjects performed an attention-enhanced visual field localizer paradigm (Fig. 5a) implemented using Presentation (Neurobehavioral Systems, Version 18.0) as part of a larger study investigating the role of visual areas for higher cognitive functions. The task consisted of a series of flickering black-and-white-colored round shaped checkerboard stimuli (flicker frequency = 7.5 Hz). Checkerboard stimuli appeared randomly for 2000 ms at one of four different locations (standard trial). Each location mapped a homologous position in one of the four visual quadrants. The regular inter-trial interval (ITI) was 0 ms. However, once every 10–14 trials (11 times overall), the ITI increased to 2000 ms (prolonged ITI) (Fig. 5b). Our paradigm featured a simple target-detection task. During 36 trials, the two centrally located squares of the checkerboard changed their color to yellow for 133 ms (target trial). Participants had to press a response box button with their left thumb as quickly as possible if they detected a target. The paradigm consisted of a total of 144 trials: 36 target trials, 108 standard trials both equally distributed across the four locations (Fig. 5b). This target probability of 25% resulted in one target trial every fourth trial on average (range 3–5 trials) (Fig. 5b). Throughout the task a black, x-shaped fixation cross was displayed at the center of the screen. Participants were instructed to continuously fixate on the fixation cross. Before the first trial, only the fixation cross was displayed for 10 s. After the last trial, only the fixation cross was displayed for 20 s. The total duration of the paradigm was 340 s (Fig. 5b). For the purpose of our analyses we defined a total of four conditions, one for each of the four stimulus locations. Each participant practiced the task prior to the measurement.

**Acquisition and analysis of fMRI data.** We acquired functional MRI data on a Siemens 3T MAGNETOM Trio scanner at the Goethe University Brain Imaging Centre using a gradient-echo 2D EPI sequence (32 axial slices, TR = 2000 ms, TE = 30 ms, FA = 90°, FoV = 192 × 192 mm<sup>2</sup>, voxel size = 3 × 3 × 3 mm<sup>3</sup>, gap = 1 mm, effective slice thickness = 4 mm). Slices were positioned parallel to the anterior- and posterior commissure. Functional images were acquired in a single run comprising the acquisition of 170 volumes. Immediately before each functional run, 6 volumes of this 2D EPI sequence were acquired with identical parameters except for a switch of phase encoding direction (posterior to anterior instead of anterior to posterior) for EPI distortion correction. Anatomical MRI data for cortex reconstruction and co-registration with functional MRI data was acquired with a high-resolution T1-weighted 3D volume using a Magnetization-Prepared Rapid Gradient-Echo (MP-RAGE) sequence (192 sagittal slices, TR = 1900 ms, TE = 3.04 ms, TI 900 ms, FA = 9°, FoV = 256 × 256 mm<sup>2</sup>, voxel size = 1 × 1 × 1 mm<sup>3</sup>). Stimulus presentation was constantly synchronized with the fMRI sequence. Head motion was minimized with pillows. The task was projected by a beamer onto a mirror attached on the head coil. MRI data were pre-processed and analyzed using BrainVoyager 20.6<sup>84</sup>, the NeuroElf Matlab toolbox ([www.neuroelf.net](http://www.neuroelf.net)) and custom software written in Matlab. One subject had to be excluded due to excessive intra-scan motion.

**Structural image pre-processing.** Structural data pre-processing included background cleaning, brain extraction and bias field correction to minimize image intensity inhomogeneities<sup>84</sup>. Bias field correction employed a “surface fitting” approach using singular value decomposition based least squares low-order (Legendre) polynomials to model low-frequency variations across 3D image space<sup>85</sup>. We used polynomials with an order of three, which we fitted to a subset of voxels labeled as belonging to white matter. The estimated parameters of the polynomials were used to construct a bias field, which was removed from the data. Our approach comprised of one iteration using automatic white matter labeling<sup>86</sup> and four iterations using manual white matter labeling.

Subsequently, structural data were transformed into Talairach coordinate space<sup>29</sup>. This comprised manual labeling of the anterior commissure (AC) and posterior commissure (PC) as well as the borders of the cerebrum. These landmarks were then used to rotate each brain in the AC-PC plane followed by piece-wise, linear transformations to fit each brain in the common Talairach “proportional grid” system<sup>19</sup>. Transformation into Talairach coordinate space was performed because the subsequent automatic segmentation procedure exploits anatomical knowledge for initial brain segmentation including removal of subcortical structures and disconnection of cortical hemispheres<sup>87</sup>. To prepare the data for this procedure, we performed a manual filling of the lateral ventricles. Based on the automatic segmentation of the structural scans along the white–gray matter boundary<sup>87</sup>, cortical hemispheres were reconstructed into folded, topologically correct mesh representations, which were tessellated to produce surface reconstructions and calculate curvature maps reflecting individual cortical folding patterns.





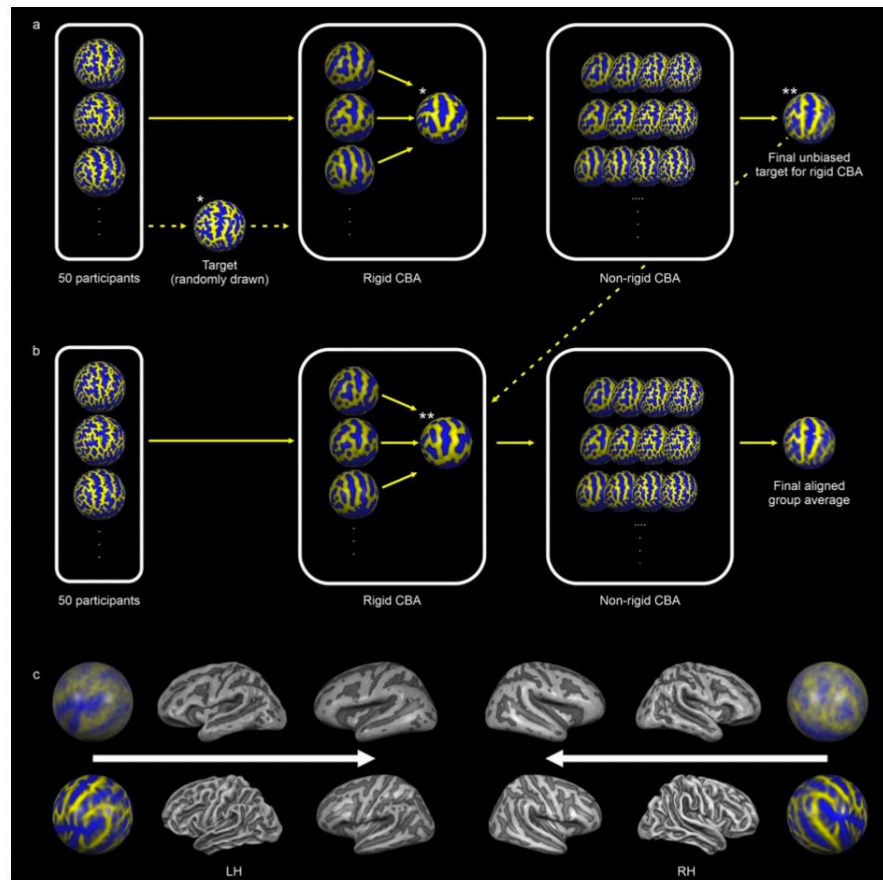


**Figure 6.** Fully data-driven CBA approach. CBA consisted of a rigid alignment to a single target brain and a non-linear alignment to an iteratively updated group average brain. (a) We carried out an initial CBA solely to generate an unbiased average target brain for the final CBA. We used a randomly selected brain from among all participants for the initial rigid CBA. (b) For the final CBA we used the unbiased average target brain created during the initial CBA for rigid CBA. (c) We generated average surface representations before and after macroanatomical alignment for each hemisphere, which we subsequently merged, inflated and used for analysis and visualization of the appropriate data sets. The upper row depicts group average spherical, folded and inflated mesh representations before applying CBA. The lower row depicts group average spherical, folded and inflated mesh representations after applying CBA.

Surface reconstructions were subsequently morphed into distortion corrected spherical representations. Finally, both folded and spherical mesh representations were downsampled to a standard number of vertices (40,962 vertices per hemisphere, mean vertex distance: 1.5 mm). We used these standardized mesh representations for all surface-based processing steps.

**Cortex-based alignment of structural data.** We then applied a high-resolution, multiscale cortex-based alignment procedure based on the individual curvature maps of all 50 participants for each hemisphere separately. This CBA approach, which reliably aligns corresponding gyri and sulci across subjects<sup>84</sup>, consists of an initial rigid and a subsequent non-rigid alignment step<sup>19</sup> (Fig. 6a,b). During the initial step, cortical folding patterns of each sphere are aligned rigidly to the cortical folding pattern of a single target sphere by global rotation. Rigid CBA operates solely on highly smoothed curvature maps containing only the most prominent anatomical landmarks. We used the rotation parameters with the highest degree of overlap between the curvature of each individual sphere and the target sphere as the starting point for the subsequent non-rigid CBA.

Non-rigid CBA employs a coarse-to-fine matching strategy, which operates sequentially at four levels of curvature smoothing, starting with the detail level used during rigid CBA. Each subsequent level includes increasingly finer anatomical details up to almost the full curvature information. Importantly, non-rigid CBA aligns each cortical folding pattern to a dynamically updated group average through iterative morphing. This moving target approach, which generates the target curvature map from the average curvature across all hemispheres at a given alignment stage avoids the possible confounding effects of a suboptimal selection of an individual target brain, whose folding pattern might deviate considerably from the cohort average.

Notably, rigid CBA typically utilizes a single brain randomly drawn from the full cohort as its target brain. However, the folding pattern of this brain might also deviate considerably from cohort average. To also address this potential confound, we first conducted a preliminary CBA encompassing both rigid and non-rigid macro-anatomical alignment (Fig. 6a). We then conducted a second, final CBA. Here, we used the aligned average brain derived from the preliminary CBA as an unbiased target for the rigid alignment step (Fig. 6b). After the final non-rigid CBA, we merged both hemispheres of each individual brain to create a global surface-based analysis space.

Furthermore, for each hemisphere we created average surface representations from the original, non-aligned folded mesh representations, which we subsequently merged, inflated and used for data analysis and visualization. We repeated these steps after applying the transformation matrix of the final rigid and non-rigid CBA to the folded mesh representations, yielding an accurate representation of the structural effects of macroanatomical alignment (Fig. 6c).

**Functional image pre-processing.** The first four volumes of each functional run were discarded to allow for T1 equilibration. Initial volume-based pre-processing of functional MRI data comprised slice timing correction using sinc interpolation and 3D motion correction using sinc interpolation. Next, we performed echo-planar imaging distortion correction using the Correction based on Opposite Phase Encoding method<sup>88,89</sup>. EPI distortion corrected functional data were co-registered to the untransformed extracted brains. This was accomplished utilizing a boundary-based registration algorithm optimized for surface-based analyses<sup>90</sup>. After co-registration to the fully cleaned but untransformed structural data, functional data were transformed into Talairach coordinate space by applying the transformation matrix generated during Talairach transformation of the structural data using sinc interpolation. This transformation preserved the original voxel size of the functional data ( $3 \times 3 \times 3 \text{ mm}^3$ ) (Fig. 7).

**Surface-based pre-processing.** The volumetric functional data were then transformed into surface space by sampling on the individual cortical surface reconstructions incorporating data from  $-1$  to  $+3 \text{ mm}$  along vertex normals using trilinear interpolation. Subsequent pre-processing of fMRI data in surface space started with spatial smoothing using a nearest neighbor interpolation (1 iteration). Based on the standardized vertex distance of  $1.5 \text{ mm}$  this approximates a 2D Gaussian smoothing kernel with a full width at half maximum (FWHM) of  $3 \text{ mm}$ . We opted for minimal spatial smoothing to prevent a loss of accuracy for our visual field localizer. Spatial smoothing was followed by linear trend removal and temporal high-pass filtering using fast Fourier transformation (high-pass  $0.00903 \text{ Hz}$ ). Based on the vertex-to-vertex referencing from the folded, topologically correct surface reconstructions to the spherical representations, we mapped the fully pre-processed functional data into a common spherical coordinate system (Fig. 7). Finally, we applied surface-based anatomical masks that only included cortical vertices in our analysis to the functional data. These masks excluded subcortical structures, which mapped onto the midline of our surface reconstructions, i.e., parts of thalamus and the basal ganglia. For functional data analysis and subsequent Bonferroni correction in surface space, this yielded a total number of 76,132 vertices.

**Full volume-based pre-processing.** To generate a purely volumetric data set for the comparison of VBA and SBAV, pre-processing after EPI distortion correction was also conducted in volume space mirroring as closely as possible the steps and parameters outlined above for surface-based pre-processing. First, we applied spatial smoothing using a 3D Gaussian smoothing kernel with a FWHM of  $3 \text{ mm}$ , which approximates the degree of surface-based spatial smoothing. Second, we applied linear trend removal and temporal high-pass filtering using fast Fourier transformation (high-pass  $0.00903 \text{ Hz}$ ) using parameters exactly matching surface-based pre-processing (Fig. 7). This data set was not transformed into surface space and did not include an anatomical mask. For functional data analysis and subsequent Bonferroni correction in volume space, this yielded a total number of 52,504 voxels. Thus, the analysis space for VBA was 69% the size of the analysis space for SBAV and CBA (52,504 voxels vs. 76,132 vertices). This difference led to a less strict Bonferroni corrected statistical threshold for VBA ( $p = 0.00000095$ ) compared to SBAV and CBA ( $p = 0.00000066$ ). Notably, we did not correct for this difference, even though it increased the difficulty of confirming the hypothesized superiority of CBA compared to VBA at the group-level.

**Comparison of functional data sets.** Overall, we generated three different functional data sets: a volume-based data set, which was entirely pre-processed and aligned in volume-space (VBA); a surface-based data set, for which the final pre-processing steps—spatial smoothing and temporal filtering—were only applied after transformation in surface space, but without macroanatomical alignment (SBAV); and a surface-based data set, which was pre-processed in exactly the same way as the SBAV data set and also utilized macroanatomical alignment (CBA) (Fig. 7). Accordingly, the primary analysis of these datasets was carried out in volume space (VBA) and surface space (SBAV, CBA) respectively. Planned direct comparisons between these three data sets allowed us to evaluate the effects of different steps of our macroanatomical alignment approach. We compared the VBA and SBAV data sets to assess in isolation the impact of surface-based pre-processing, while keeping macro-

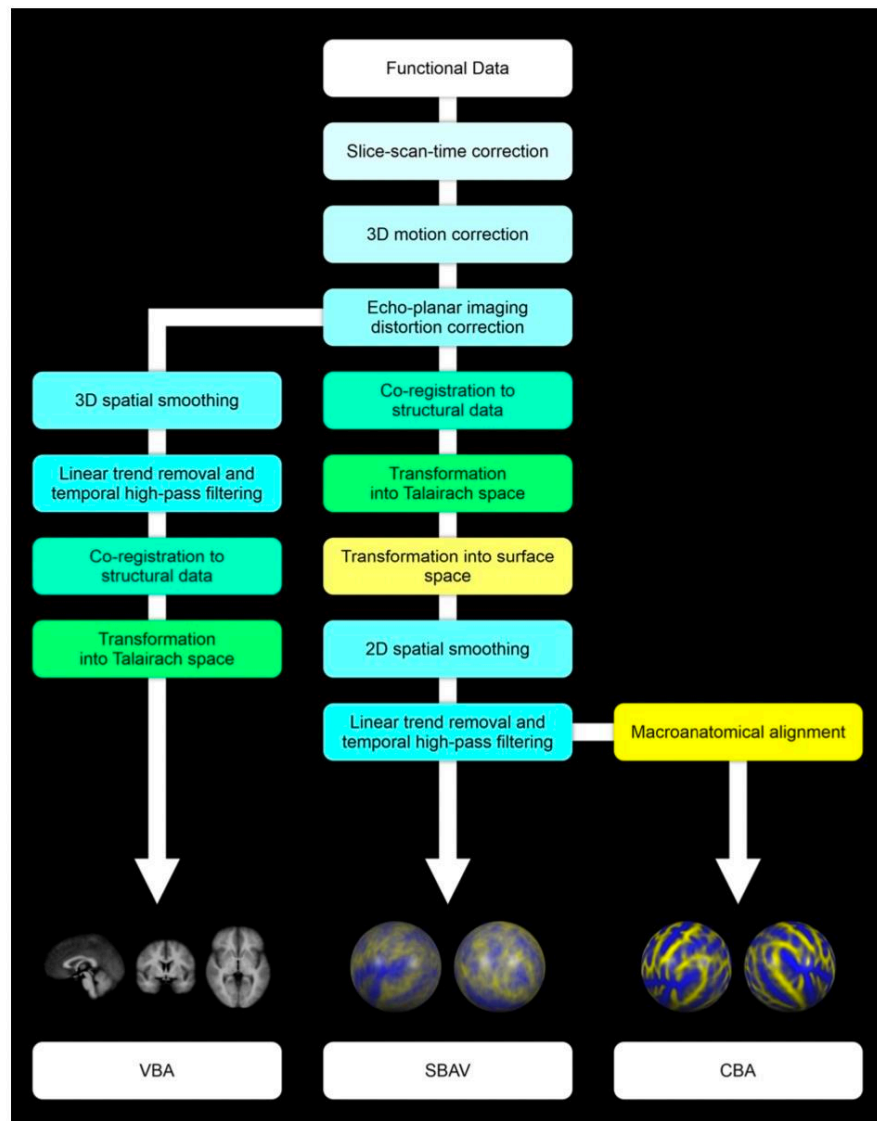


**Figure 7.** Sequences of functional data pre-processing, coregistration of structural and functional data and spatial transformation operations used to generate the three functional data sets used in our study: VBA, SBAV and CBA. For VBA we conducted all data pre-processing operations in volume space, including slice-scan-time correction, 3D motion correction, echo-planar imaging distortion correction, 3D spatial smoothing and linear trend removal with temporal high-pass filtering. Finally, functional data were co-registered to the structural data and transformed into Talairach space. For SBAV and CBA, we conducted all data pre-processing operations up to echo-planar imaging distortion correction in volume space. Here, co-registration of functional data to the structural data and transformation into Talairach space was followed by transformation into surface space. We then conducted 2D spatial smoothing and linear trend removal with temporal high-pass filtering in surface space. For CBA only, we subsequently applied macroanatomical alignment.

anatomical alignment constant. We compared the SBAV and CBA data sets to assess in isolation the impact of macroanatomical alignment while keeping pre-processing parameters constant. Finally, we compared the VBA and CBA data sets to assess the combined impact of both surface-based pre-processing and macroanatomical alignment.

**fMRI group analysis of visual quadrants.** We performed multi-subject statistical analyses using multiple linear regression of the BOLD signal. The presentation of each checkerboard stimulus sequence at a single location was modelled by an ideal box-car function, which covered the volume of each trial, convolved with a synthetic two-gamma function. These predictors were used to build the design matrix of the experiment. Individual statistical maps were generated by associating each voxel with the beta-value corresponding to the specific set of predictors and calculated on the basis of the least mean squares solution of the general linear model. The resulting individual statistical maps were entered into a second-level random-effects group analysis using a summary statistic approach.

We performed analyses focusing on the mapping of the four visual quadrants at the group level. To define group-level ROIs for each visual quadrant, we computed separate weighted contrasts for each quadrant against the other three quadrants. We assigned a weight of three to the position of interest, e.g.  $(\beta_{Quad_1} \times 3) / (\beta_{Quad_2} + \beta_{Quad_3} + \beta_{Quad_4})$  ( $p < 0.05$ , Bonferroni corrected). This allowed us to detect brain regions showing significant position selectivity. For each resulting group-level ROI, we extracted average time courses (incl. standard errors of the mean) for all four conditions. We conducted this analysis for all three data sets (VBA, SBAV, CBA). For the VBA data set, we computed this analysis fully in volume space using the original resolution of the functional data (voxel size:  $3 \times 3 \times 3$  mm<sup>3</sup>). We projected the resulting maps on the non-aligned average surface representation, i.e. the inflated mesh representations before CBA, as depicted in the upper row of Fig. 6c. To this end, volumetric functional maps were transformed into surface space by sampling on the average cortical surface incorporating data from  $-1$  to  $+3$  mm along vertex normals of the group average surface brain using trilinear interpolation.

With this transformation we aimed to achieve a visualization and quantification of VBA results equivalent to the SBAV and CBA results. To make all three data sets comparable, this transformation of volumetric functional maps closely mirrored the transformation of functional data into surface space conducted for the SBAV and CBA data sets during pre-processing. Thus, we were able to assess cluster sizes for all ROIs of all data sets in surface space based on the number vertices. We also extracted the number of voxels for the VBA results before transformation into surface space. However, this parameter is not suitable for a comparison with the other data sets and was only included to ensure a comprehensive reporting of our findings.

We used two approaches to determine, whether position selectivity differed between our three data sets: first, to assess differences in the extent of early visual cortex showing significant position selectivity, we compared ROI size, i.e. the number of vertices, for each position of interest across data sets. To this end, we compared quantitative changes in group ROI size between alignment methods utilizing the following formula:  $\{(\text{size\_ROI}_{Quad}[AM_m] - \text{size\_ROI}_{Quad}[AM_n]) / \text{size\_ROI}_{Quad}[AM_n]\} \times 100$ . Here, Quad indexes the visual quadrant of interest (LR, LL, UL, UR). AM refers to alignment methods (VBA, SBAV, CBA). The subscripted characters n and m specify AMs, with m referring to the less advanced AM and n referring to the comparatively more advanced AM. Accordingly, a positive value indicates an increase in ROI size—and hence position selectivity—for the more advanced alignment method. Second, to test whether the strength of position selectivity within the ROIs of each visual quadrant changed across alignment techniques, we conducted separate linear mixed models with random intercept for each visual quadrant using R (version R 4.1.2). To calculate the degree of position selectivity within each ROI, we contrasted the single-subject t-values of each visual quadrant (“position of interest”) against the single-subject t-values of the three other visual quadrants, e.g.  $(t_{Quad_1} \times 3) / (t_{Quad_2} + t_{Quad_3} + t_{Quad_4})$ , separately for each alignment method. We used the results of these contrasts of each subject as the dependent variable and the alignment methods (VBA, SBAV and CBA) as the independent variable. To correct for multiple comparisons, p values were adjusted using Bonferroni correction. Thus, a significant effect in the linear mixed models would indicate a relevant change in position selectivity across alignment methods for a given visual quadrant.

Finally, to assess the impact of the three alignment approaches on horizontal and vertical symmetry of our group-level ROIs, we computed an established asymmetry index (AI)<sup>91</sup> based on ROI size, i.e. the number of vertices, between each pair of ROIs using the following formula:  $(\text{size}_{ROI_1} - \text{size}_{ROI_2}) / (\text{size}_{ROI_1} + \text{size}_{ROI_2}) \times 100$ . For calculating the vertical AI, we compared the number of vertices of ROIs facing each other at the vertical axis. Thus, for the vertical AI we compared left and right visual quadrants. For calculating the horizontal AI, we compared the number of vertices of ROIs facing each other at the horizontal axis. Thus, for the horizontal AI we compared upper and lower visual quadrants.

**Probability maps.** To quantify and visualize variability of functional activation and possible changes induced by macroanatomical alignment, the use of PMs has been proposed. PMs are specifically useful to assess inconsistencies, i.e., disparities between individuals regarding the location of a particular (visual) area<sup>92,93</sup>. To quantify the spatial consistency of position selective activation patterns, we generated PMs for each visual quadrant for all three data sets (VBA, SBAV, CBA). These maps represent the relative number of subjects showing significant task-related activity in our single-subject analysis. To this end, we generated single-subject t-maps based on the same weighted contrasts employed in the group analysis but set at a more lenient statistical threshold ( $p < 0.05$  uncorrected). PMs were calculated by counting the number of subjects showing above-threshold activation in their individual t-maps at a given vertex, dividing this value by the total number of subjects, and multiplying the result by 100. For the VBA data set, we computed all of these steps in volume space and transformed the final PM into surface space using the same parameters outlined above for the volumetric group

maps. Finally, we thresholded all PMs at a minimum of 10% probability of activation overlap. We also applied a cluster level threshold of 100 vertices to focus on the main areas of interest, i.e., the visual quadrants. Additionally, we counted the number of vertices in the corresponding probability maps exceeding the threshold of 10% probability of activation overlap for each visual quadrant and analysis methods. Our goal was to quantify and compare the extent of early visual cortex, where each analysis method had a relevant impact on the probability of activation overlap.

**Probability difference maps.** Additionally, we aimed to quantify changes in spatial consistency of position selective activation patterns resulting from the different alignment methods. To this end, we calculated PDMs for each visual quadrant, thresholded at a minimum probability difference of 5%, using the original unthresholded PMs. The resulting three PDMs capture different aspects of our overall approach: the impact of surface-based functional data readout and pre-processing compared to volume-based alignment (SBAV minus VBA), the additional impact of applying macroanatomical alignment (CBA minus SBAV) and the additive impact of both methods (CBA minus VBA). Moreover, we counted the number of vertices in the corresponding PDMs exceeding the threshold of plus five or minus five % difference in probability of activation overlap for each visual quadrant. Our goal was to quantify and compare the extent of early visual cortex, where we observed a difference in the probability of activation overlap, for a comparison of analysis method.

**Single-subject ROI peak vertex distribution mapping.** For single-subject level analyses, we first defined ROIs for each subject independently before and after macroanatomical alignment, i.e., for SBAV and CBA, using the same weighted contrasts employed in the group analysis. We applied a more lenient statistical threshold ( $p < 0.05$  uncorrected). Next, we determined the peak vertex for each subject's four visual quadrant ROIs, i.e., the vertex with the highest t-value, for SBAV and CBA. To specifically assess the impact of macroanatomical alignment on the overlap of single-subject ROI peak vertices for each visual quadrant, we mapped all peak vertices per visual quadrant for SBAV and CBA. To quantify changes in the number of precisely overlapping single-subject peak vertices, we counted for each occipital vertex the number of peak vertices for SBAV and CBA. We performed this analysis in addition to the PM- and PDM-analysis to provide a more direct assessment and visualization of the effects of macroanatomical alignment on the spatial correspondence of single-subject ROIs. We restricted this particular analysis to the comparison between SBAV and CBA, because we were specifically interested in studying in isolation the effect of macroanatomical alignment introduced in the CBA data set on the overlap of single-subject ROI peak vertices. Since both VBA and SBAV did not include macroanatomical alignment, but both data sets differed in a number of other pre-processing steps, the direct comparison between SBAV and CBA is the most appropriate to study this particular issue.

#### Data availability

The data that support the findings of this study are available from the corresponding author, R.A.B., upon reasonable request.

Received: 1 July 2021; Accepted: 2 August 2022

Published online: 22 August 2022

#### References

- Wandell, B. A., Dumoulin, S. O. & Brewer, A. A. Visual field maps in human cortex. *Neuron* **56**, 366–383. <https://doi.org/10.1016/j.neuron.2007.10.012> (2007).
- Corbetta, M. & Shulman, G. L. Control of goal-directed and stimulus-driven attention in the brain. *Nat. Rev. Neurosci.* **3**, 201–215. <https://doi.org/10.1038/nrn755> (2002).
- Das, M., Bennett, D. M. & Dutton, G. N. Visual attention as an important visual function: An outline of manifestations, diagnosis and management of impaired visual attention. *Br. J. Ophthalmol.* **91**, 1556–1560. <https://doi.org/10.1136/bjo.2006.104844> (2007).
- de Haan, B., Bither, M., Brauer, A. & Karnath, H. O. Neural correlates of spatial attention and target detection in a multi-target environment. *Cereb. Cortex* **25**, 2321–2331. <https://doi.org/10.1093/cercor/bhu046> (2015).
- Goodale, M. & Milner, D. One brain—two visual systems. *Psychologist* **19**, 660–663 (2006).
- Bergmann, J., Genç, E., Kohler, A., Singer, W. & Pearson, J. Neural anatomy of primary visual cortex limits visual working memory. *Cereb. Cortex* **26**, 43–50. <https://doi.org/10.1093/cercor/bhu168> (2014).
- Lee, J. *et al.* fMRI evidence of aberrant neural adaptation for objects in schizophrenia and bipolar disorder. *Hum. Brain Mapp.* **40**, 1608–1617. <https://doi.org/10.1002/hbm.24472> (2019).
- Silverstein, S. M. *et al.* An fMRI examination of visual integration in schizophrenia. *J. Integr. Neurosci.* **8**, 175–202. <https://doi.org/10.1142/s0219635209002113> (2009).
- Dumoulin, S. O. & Wandell, B. A. Population receptive field estimates in human visual cortex. *Neuroimage* **39**, 647–660. <https://doi.org/10.1016/j.neuroimage.2007.09.034> (2008).
- Sereno, M. I. *et al.* Borders of multiple visual areas in humans revealed by functional magnetic resonance imaging. *Science (New York, NY)* **268**, 889–893. <https://doi.org/10.1126/science.7754376> (1995).
- Harrison, S. A. & Tong, F. Decoding reveals the contents of visual working memory in early visual areas. *Nature* **458**, 632–635. <https://doi.org/10.1038/nature07832> (2009).
- Peters, B., Kaiser, J., Rahm, B. & Bledowski, C. Activity in human visual and parietal cortex reveals object-based attention in working memory. *J. Neurosci.* **35**, 3360–3369. <https://doi.org/10.1523/jneurosci.3795-14.2015> (2015).
- Downing, P. E., Chan, A. W., Peelen, M. V., Dodds, C. M. & Kanwisher, N. Domain specificity in visual cortex. *Cereb. Cortex* **16**, 1453–1461. <https://doi.org/10.1093/cercor/bhj086> (2006).
- Kanwisher, N., McDermott, J. & Chun, M. M. The fusiform face area: A module in human extrastriate cortex specialized for face perception. *J. Neurosci.* **17**, 4302–4311. <https://doi.org/10.1523/jneurosci.17-11-04302.1997> (1997).
- Brett, M., Johnsrude, I. S. & Owen, A. M. The problem of functional localization in the human brain. *Nat. Rev. Neurosci.* **3**, 243–249. <https://doi.org/10.1038/nrn756> (2002).

16. Desai, R., Liebenthal, E., Possing, E. T., Waldron, E. & Binder, J. R. Volumetric vs surface-based alignment for localization of auditory cortex activation. *Neuroimage* **26**, 1019–1029. <https://doi.org/10.1016/j.neuroimage.2005.03.024> (2005).
17. Dougherty, R. F. et al. Visual field representations and locations of visual areas V1/2/3 in human visual cortex. *J. Vis.* **3**, 586–598. <https://doi.org/10.1167/3.10.1> (2003).
18. Fischl, B., Sereno, M. I. & Dale, A. M. Cortical surface-based analysis. II: Inflation, flattening, and a surface-based coordinate system. *Neuroimage* **9**, 195–207. <https://doi.org/10.1006/nimg.1998.0396> (1999).
19. Frost & Goebel. Measuring structural-functional correspondence: Spatial variability of specialised brain regions after macro-anatomical alignment. *Neuroimage* **59**, 1369–1381. <https://doi.org/10.1016/j.neuroimage.2011.08.035> (2012).
20. Frost & Goebel. Functionally informed cortex based alignment: An integrated approach for whole-cortex macro-anatomical and ROI-based functional alignment. *Neuroimage* **83**, 1002–1010. <https://doi.org/10.1016/j.neuroimage.2013.07.056> (2013).
21. Steinmetz, H., Fürst, G. & Freund, H. J. Variation of perisylvian and calcarine anatomic landmarks within stereotaxic proportional coordinates. *Am. J. Neuroradiol.* **11**, 1123–1130 (1990).
22. Van Essen, D. C. et al. An integrated software suite for surface-based analyses of cerebral cortex. *J. Am. Med. Inform. Assoc.* **8**, 443–459. <https://doi.org/10.1136/jamia.2001.0080443> (2001).
23. Zilles, K. et al. Quantitative analysis of sulci in the human cerebral cortex: Development, regional heterogeneity, gender difference, asymmetry, intersubject variability and cortical architecture. *Hum. Brain Mapp.* **5**, 218–221. [https://doi.org/10.1002/\(SICI\)1097-0193\(1997\)5:4%3c218::AID-HBM2%3e3.0.CO;2-6](https://doi.org/10.1002/(SICI)1097-0193(1997)5:4%3c218::AID-HBM2%3e3.0.CO;2-6) (1997).
24. Bridge, H. Mapping the visual brain: How and why. *Eye (Lond)* **25**, 291–296. <https://doi.org/10.1038/eye.2010.166> (2011).
25. Fedorenko, E., Hsieh, P. J., Nieto-Castañón, A., Whitfield-Gabrieli, S. & Kanwisher, N. New method for fMRI investigations of language: Defining ROIs functionally in individual subjects. *J. Neurophysiol.* **104**, 1177–1194. <https://doi.org/10.1152/jn.00032.2010> (2010).
26. Julian, J. B., Fedorenko, E., Webster, J. & Kanwisher, N. An algorithmic method for functionally defining regions of interest in the ventral visual pathway. *Neuroimage* **60**, 2357–2364. <https://doi.org/10.1016/j.neuroimage.2012.02.055> (2012).
27. Nieto-Castañón, A. & Fedorenko, E. Subject-specific functional localizers increase sensitivity and functional resolution of multi-subject analyses. *Neuroimage* **63**, 1646–1669. <https://doi.org/10.1016/j.neuroimage.2012.06.065> (2012).
28. Smith, S. M. et al. Functional connectomics from resting-state fMRI. *Trends Cogn. Sci.* **17**, 666–682. <https://doi.org/10.1016/j.tics.2013.09.016> (2013).
29. Talairach, J. & Tournoux, P. *Co-planar Stereotaxic Atlas of the Human Brain: 3-Dimensional Proportional System: An Approach to Cerebral Imaging* (Thieme, 1988).
30. Evans, A. C. et al. 3D statistical neuroanatomical models from 305 MRI volumes. In *1993 IEEE Conference Record Nuclear Science Symposium and Medical Imaging Conference*, 1813–1817 vol.1813 (1993).
31. Klein, A. et al. Evaluation of volume-based and surface-based brain image registration methods. *Neuroimage* **51**, 214–220. <https://doi.org/10.1016/j.neuroimage.2010.01.091> (2010).
32. Ghosh, S. S. et al. Evaluating the validity of volume-based and surface-based brain image registration for developmental cognitive neuroscience studies in children 4 to 11 years of age. *Neuroimage* **53**, 85–93. <https://doi.org/10.1016/j.neuroimage.2010.05.075> (2010).
33. Nieto-Castañón, A., Ghosh, S. S., Tourville, J. A. & Guenther, F. H. Region of interest based analysis of functional imaging data. *Neuroimage* **19**, 1303–1316. [https://doi.org/10.1016/s1053-8119\(03\)00188-5](https://doi.org/10.1016/s1053-8119(03)00188-5) (2003).
34. Fischl, B., Sereno, M. I., Tootell, R. B. & Dale, A. M. High-resolution intersubject averaging and a coordinate system for the cortical surface. *Hum. Brain Mapp.* **8**, 272–284. [https://doi.org/10.1002/\(sici\)1097-0193\(1999\)8:4%3c272::aid-hbm10%3e3.0.co;2-4](https://doi.org/10.1002/(sici)1097-0193(1999)8:4%3c272::aid-hbm10%3e3.0.co;2-4) (1999).
35. Brodoehl, S., Gaser, C., Dahnke, R., Witte, O. W. & Klingner, C. M. Surface-based analysis increases the specificity of cortical activation patterns and connectivity results. *Sci. Rep.* **10**, 5737. <https://doi.org/10.1038/s41598-020-62832-z> (2020).
36. Fischl, B. et al. Cortical folding patterns and predicting cytoarchitecture. *Cereb. Cortex* **18**, 1973–1980. <https://doi.org/10.1093/cercor/bhm225> (2008).
37. Anticevic, A. et al. Comparing surface-based and volume-based analyses of functional neuroimaging data in patients with schizophrenia. *Neuroimage* **41**, 835–848. <https://doi.org/10.1016/j.neuroimage.2008.02.052> (2008).
38. Pantazis, D. et al. Comparison of landmark-based and automatic methods for cortical surface registration. *Neuroimage* **49**, 2479–2493. <https://doi.org/10.1016/j.neuroimage.2009.09.027> (2010).
39. Van Essen, D. C. & Drury, H. A. Structural and functional analyses of human cerebral cortex using a surface-based atlas. *J. Neurosci.* **17**, 7079–7102. <https://doi.org/10.1523/jneurosci.17-18-07079.1997> (1997).
40. Frost, M. A., Esposito, F. & Goebel, R. Improved correspondence of resting-state networks after macroanatomical alignment. *Hum. Brain Mapp.* **35**, 673–682. <https://doi.org/10.1002/hbm.22191> (2014).
41. Hinds, O. P. et al. Accurate prediction of V1 location from cortical folds in a surface coordinate system. *Neuroimage* **39**, 1585–1599. <https://doi.org/10.1016/j.neuroimage.2007.10.033> (2008).
42. Weiner, K. S. et al. Defining the most probable location of the parahippocampal place area using cortex-based alignment and cross-validation. *Neuroimage* **170**, 373–384. <https://doi.org/10.1016/j.neuroimage.2017.04.040> (2018).
43. Rosenke, M., van Hoof, R., van den Hurk, J., Grill-Spector, K. & Goebel, R. A probabilistic functional atlas of human occipito-temporal visual cortex. *Cereb. Cortex* <https://doi.org/10.1093/cercor/bhaa246> (2020).
44. Huang, T., Chen, X., Jiang, J., Zhen, Z. & Liu, J. A probabilistic atlas of the human motion complex built from large-scale functional localizer data. *Hum. Brain Mapp.* **40**, 3475–3487. <https://doi.org/10.1002/hbm.24610> (2019).
45. Di Russo, F., Martinez, A. & Hillyard, S. A. Source analysis of event-related cortical activity during visuo-spatial attention. *Cereb. Cortex* **13**, 486–499. <https://doi.org/10.1093/cercor/13.5.486> (2003).
46. Di Russo, F., Martinez, A., Sereno, M. I., Pitzalis, S. & Hillyard, S. A. Cortical sources of the early components of the visual evoked potential. *Hum. Brain Mapp.* **15**, 95–111. <https://doi.org/10.1002/hbm.10010> (2002).
47. Shighihara, Y., Hoshi, H. & Zeki, S. Early visual cortical responses produced by checkerboard pattern stimulation. *Neuroimage* <https://doi.org/10.1016/j.neuroimage.2016.03.078> (2016).
48. Kraft, A. et al. fMRI localizer technique: Efficient acquisition and functional properties of single retinotopic positions in the human visual cortex. *Neuroimage* **28**, 453–463. <https://doi.org/10.1016/j.neuroimage.2005.05.050> (2005).
49. Bressler, D. W. & Silver, M. A. Spatial attention improves reliability of fMRI retinotopic mapping signals in occipital and parietal cortex. *Neuroimage* **53**, 526–533. <https://doi.org/10.1016/j.neuroimage.2010.06.063> (2010).
50. Anderson, J., Cameron, E. & Levine, M. A method for quantifying visual field inhomogeneities. *Vis. Res.* **105**, 25. <https://doi.org/10.1016/j.visres.2014.09.010> (2014).
51. Liu, T., Heeger, D. J. & Carrasco, M. Neural correlates of the visual vertical meridian asymmetry. *J. Vis.* **6**, 1294–1306. <https://doi.org/10.1167/6.11.12> (2006).
52. O'Connell, C. et al. Structural and functional correlates of visual field asymmetry in the human brain by diffusion kurtosis MRI and functional MRI. *NeuroReport* **27**, 1225–1231. <https://doi.org/10.1097/wnr.0000000000000682> (2016).
53. Rubin, N., Nakayama, K. & Shapley, R. Enhanced perception of illusory contours in the lower versus upper visual hemifields. *Science* **271**, 651–653. <https://doi.org/10.1126/science.271.5249.651> (1996).
54. Bullmore, E. & Sporns, O. Complex brain networks: Graph theoretical analysis of structural and functional systems. *Nat. Rev. Neurosci.* **10**, 186–198. <https://doi.org/10.1038/nrn2575> (2009).

55. Chen, H., Yao, D. & Liu, Z. A study on asymmetry of spatial visual field by analysis of the fMRI BOLD response. *Brain Topogr.* **17**, 39–46. <https://doi.org/10.1023/b:brat.0000047335.00110.6a> (2004).
56. Loughnane, G. M., Shanley, J. P., Lalor, E. C. & O'Connell, R. G. Behavioral and electrophysiological evidence of opposing lateral visuospatial asymmetries in the upper and lower visual fields. *Cortex* **63**, 220–231. <https://doi.org/10.1016/j.cortex.2014.09.003> (2015).
57. Eickhoff, S. B., Rottschy, C., Kujovic, M., Palomero-Gallagher, N. & Zilles, K. Organizational principles of human visual cortex revealed by receptor mapping. *Cereb. Cortex* **18**, 2637–2645. <https://doi.org/10.1093/cercor/bhh024> (2008).
58. Curcio, C. A. & Allen, K. A. Topography of ganglion cells in human retina. *J. Comp. Neurol.* **300**, 5–25. <https://doi.org/10.1002/cne.903000103> (1990).
59. Silson, E. H., Reynolds, R. C., Kravitz, D. J. & Baker, C. I. Differential sampling of visual space in ventral and dorsal early visual cortex. *J. Neurosci.* **38**, 2294–2303. <https://doi.org/10.1523/jneurosci.2717-17.2018> (2018).
60. Hagler, D. J. Jr. Visual field asymmetries in visual evoked responses. *J. Vis.* **14**, 13. <https://doi.org/10.1167/14.14.13> (2014).
61. Schmidtman, G., Logan, A. J., Kennedy, G. J., Gordon, G. E. & Loffler, G. Distinct lower visual field preference for object shape. *J. Vis.* **15**, 18. <https://doi.org/10.1167/15.5.18> (2015).
62. Thomas, N. A. & Elias, L. J. Upper and lower visual field differences in perceptual asymmetries. *Brain Res.* **1387**, 108–115. <https://doi.org/10.1016/j.brainres.2011.02.063> (2011).
63. Zito, G. A., Cazzoli, D., Müri, R. M., Mosimann, U. P. & Nef, T. Behavioral differences in the upper and lower visual hemifields in shape and motion perception. *Front. Behav. Neurosci.* **10**, 128–128. <https://doi.org/10.3389/fnbeh.2016.00128> (2016).
64. Bakroon, A. & Lakshminarayanan, V. Visual function in autism spectrum disorders: A critical review. *Clin. Exp. Optim.* **99**, 297–308. <https://doi.org/10.1111/cxo.12383> (2016).
65. Butler, P. D. *et al.* Dysfunction of early-stage visual processing in schizophrenia. *Am. J. Psychiatry* **158**, 1126–1133. <https://doi.org/10.1176/appi.ajp.158.7.1126> (2001).
66. Butler, P. D., Silverstein, S. M. & Dakin, S. C. Visual perception and its impairment in schizophrenia. *Biol. Psychiatry* **64**, 40–47. <https://doi.org/10.1016/j.biopsych.2008.03.023> (2008).
67. Chen, C. Y. *et al.* Visual spatial attention in children with attention deficit hyperactivity disorder. *Chang Gung Med. J.* **25**, 514–521 (2002).
68. Hale, T. S. *et al.* Visual network asymmetry and default mode network function in ADHD: An fMRI study. *Front. Psychiatry* **5**, 81. <https://doi.org/10.3389/fpsy.2014.00081> (2014).
69. Sanz-Cervera, P., Pastor-Cerezuola, G., González-Sala, F., Tarraga-Minguez, R. & Fernández-Andrés, M.-I. Sensory processing in children with autism spectrum disorder and/or attention deficit hyperactivity disorder in the home and classroom contexts. *Front. Psychol.* **8**, 1772–1772. <https://doi.org/10.3389/fpsyg.2017.01772> (2017).
70. Seymour, R. A., Rippon, G., Gooding-Williams, G., Schoffelen, J. M. & Kessler, K. Dysregulated oscillatory connectivity in the visual system in autism spectrum disorder. *Brain* **142**, 3294–3305. <https://doi.org/10.1093/brain/awz214> (2019).
71. Shimizu, V. T., Bueno, O. F. & Miranda, M. C. Sensory processing abilities of children with ADHD. *Braz. J. Phys. Ther.* **18**, 343–352. <https://doi.org/10.1590/bjpt-rbf.2014.0043> (2014).
72. Bittner, R. A. *et al.* The when and where of working memory dysfunction in early-onset schizophrenia—a functional magnetic resonance imaging study. *Cereb. Cortex* **25**, 2494–2506. <https://doi.org/10.1093/cercor/bhu050> (2015).
73. Butler, P. D., Thompson, J. L., Seitz, A. R., Deveau, J. & Silverstein, S. M. Visual perceptual remediation for individuals with schizophrenia: Rationale, method, and three case studies. *Psychiatr. Rehabil. J.* **40**, 43–52. <https://doi.org/10.1037/prj0000212> (2017).
74. Haenschel, C. *et al.* Contribution of impaired early-stage visual processing to working memory dysfunction in adolescents with schizophrenia: A study with event-related potentials and functional magnetic resonance imaging. *Arch. Gen. Psychiatry* **64**, 1229–1240. <https://doi.org/10.1001/archpsyc.64.11.1229> (2007).
75. Manoach, D. S. Prefrontal cortex dysfunction during working memory performance in schizophrenia: Reconciling discrepant findings. *Schizophr. Res.* **60**, 285–298. [https://doi.org/10.1016/s0920-9964\(02\)00294-3](https://doi.org/10.1016/s0920-9964(02)00294-3) (2003).
76. French, L. & Paus, T. A FreeSurfer view of the cortical transcriptome generated from the Allen Human Brain Atlas. *Front. Neurosci.* <https://doi.org/10.3389/fnins.2015.00323> (2015).
77. Gulban, O. F. *et al.* Improving a probabilistic cytoarchitectonic atlas of auditory cortex using a novel method for inter-individual alignment. *Elife* **9**, e56963. <https://doi.org/10.7554/eLife.56963> (2020).
78. Hawrylycz, M. J. *et al.* An anatomically comprehensive atlas of the adult human brain transcriptome. *Nature* **489**, 391–399. <https://doi.org/10.1038/nature11405> (2012).
79. Sabuncu, M. R. *et al.* Function-based intersubject alignment of human cortical anatomy. *Cereb. Cortex* **20**, 130–140. <https://doi.org/10.1093/cercor/bhp085> (2009).
80. Conroy, B. R., Singer, B. D., Guntupalli, J. S., Ramadge, P. J. & Haxby, J. V. Inter-subject alignment of human cortical anatomy using functional connectivity. *Neuroimage* **81**, 400–411. <https://doi.org/10.1016/j.neuroimage.2013.05.009> (2013).
81. Glasser, M. F. *et al.* A multi-modal parcellation of human cerebral cortex. *Nature* **536**, 171–178. <https://doi.org/10.1038/nature18933> (2016).
82. Gulban, O. F. *et al.* Improving a probabilistic cytoarchitectonic atlas of auditory cortex using a novel method for inter-individual alignment. *Elife* **9**, 25. <https://doi.org/10.7554/eLife.56963> (2020).
83. Oldfield, R. C. The assessment and analysis of handedness: The Edinburgh inventory. *Neuropsychologia* **9**, 97–113. [https://doi.org/10.1016/0028-3932\(71\)90067-4](https://doi.org/10.1016/0028-3932(71)90067-4) (1971).
84. Goebel, R., Esposito, F. & Formisano, E. Analysis of functional image analysis contest (FIAC) data with brainvoyager QX: From single-subject to cortically aligned group general linear model analysis and self-organizing group independent component analysis. *Hum. Brain Mapp.* **27**, 392–401. <https://doi.org/10.1002/hbm.20249> (2006).
85. Sled, J. G., Zijdenbos, A. P. & Evans, A. C. In *Proceedings of the 15th International Conference on Information Processing in Medical Imaging* 459–464 (Springer-Verlag, 1997).
86. Hou, Z., Huang, S., Hu, Q. & Nowinski, W. L. A fast and automatic method to correct intensity inhomogeneity in MR brain images. *Med. Image Comput. Assist. Interv.* **9**, 324–331. [https://doi.org/10.1007/11866763\\_40](https://doi.org/10.1007/11866763_40) (2006).
87. Kriegeskorte, N. & Goebel, R. An efficient algorithm for topologically correct segmentation of the cortical sheet in anatomical MR volumes. *Neuroimage* **14**, 329–346 (2001).
88. Fan, X. *et al.* Metabolic effects of adjunctive aripiprazole in clozapine-treated patients with schizophrenia. *Acta Psychiatr. Scand.* **127**, 217–226. <https://doi.org/10.1111/acps.12009> (2013).
89. Breman, H. *et al.* In *Biomedical Image Registration* (eds Špičlin, Ž *et al.*) 122–130 (Springer, 2020).
90. Greve, D. N. & Fischl, B. Accurate and robust brain image alignment using boundary-based registration. *Neuroimage* **48**, 63–72. <https://doi.org/10.1016/j.neuroimage.2009.06.060> (2009).
91. Heckemann, R. A. *et al.* Automatic morphometry in Alzheimer's disease and mild cognitive impairment. *Neuroimage* **56**, 2024–2037. <https://doi.org/10.1016/j.neuroimage.2011.03.014> (2011).
92. Wang, L., Mruczek, R. E., Arcaro, M. J. & Kastner, S. Probabilistic maps of visual topography in human cortex. *Cereb. Cortex* **25**, 3911–3931. <https://doi.org/10.1093/cercor/bhu277> (2015).
93. Yamamoto, H. *et al.* Inconsistency and uncertainty of the human visual area loci following surface-based registration: Probability and Entropy Maps. *Hum. Brain Mapp.* **33**, 121–129. <https://doi.org/10.1002/hbm.21200> (2012).



### Acknowledgements

The authors are most grateful to Deliah Macht, Christina Raab and Leonie Winkler-Lauble for help with data acquisition. C.V Barnes-Scheufler was supported by a “main doctus” scholarship from The Polytechnic Foundation of Frankfurt am Main. E. Raspor was supported by a Research Grant for Doctoral Programmes in Germany from the German Academic Exchange Service (DAAD).

### Author contributions

All authors made substantial contributions to the conception or design of the work, or the acquisition, analysis, or interpretation of data. A.R. and R.A.B. acquired funding. R.A.B., B.P., M.S. and L.R. designed the experiment. M.Q., C.V.B.-S., L.R. and R.A.B. acquired the data. E.R. and R.G. provided analytical tools. M.Q., C.S. and R.A.B. analyzed the data. M.Q. and R.A.B. undertook the literature searches and wrote the first draft of the manuscript. All authors contributed to and revised the manuscript. All authors read and approved the final manuscript.

### Funding

Open Access funding enabled and organized by Projekt DEAL.

### Competing interests

The authors declare no competing interests.

### Additional information

**Correspondence** and requests for materials should be addressed to R.A.B.

**Reprints and permissions information** is available at [www.nature.com/reprints](http://www.nature.com/reprints).

**Publisher's note** Springer Nature remains neutral with regard to jurisdictional claims in published maps and institutional affiliations.



**Open Access** This article is licensed under a Creative Commons Attribution 4.0 International License, which permits use, sharing, adaptation, distribution and reproduction in any medium or format, as long as you give appropriate credit to the original author(s) and the source, provide a link to the Creative Commons licence, and indicate if changes were made. The images or other third party material in this article are included in the article's Creative Commons licence, unless indicated otherwise in a credit line to the material. If material is not included in the article's Creative Commons licence and your intended use is not permitted by statutory regulation or exceeds the permitted use, you will need to obtain permission directly from the copyright holder. To view a copy of this licence, visit <http://creativecommons.org/licenses/by/4.0/>.

© The Author(s) 2022

## **Darstellung des eigenen Anteils an der Publikation (Confirmation of contributions)**

Mishal Qubad designed the study, recruited participants, acquired the data, analyzed the data, searched the literature, wrote the initial draft, created the figures, and revised the manuscript. Data acquisition included psychometric tests, blood collection and data acquisition during fMRI and MEG. Data analyses included analyses in *Brain Voyager*.

I hereby confirm these contributions.

## Literaturverzeichnis

1. Wandell BA, Dumoulin SO, Brewer AA. Visual field maps in human cortex. *Neuron*. 2007;56:366-383.
2. Bergmann J, Genç E, Kohler A, Singer W, Pearson J. Neural Anatomy of Primary Visual Cortex Limits Visual Working Memory. *Cerebral Cortex*. 2014;26:43-50.
3. Corbetta M, Shulman GL. Control of goal-directed and stimulus-driven attention in the brain. *Nature Reviews Neuroscience*. Vol 32002:201-215.
4. Das M, Bennett DM, Dutton GN. Visual attention as an important visual function: an outline of manifestations, diagnosis and management of impaired visual attention. *Br J Ophthalmol*. 2007;91:1556-1560.
5. Kelemen O, Kiss I, Benedek G, Kéri S. Perceptual and cognitive effects of antipsychotics in first-episode schizophrenia: the potential impact of GABA concentration in the visual cortex. *Prog Neuropsychopharmacol Biol Psychiatry*. 2013;47:13-19.
6. Kiss I, Fábíán A, Benedek G, Kéri S. When doors of perception open: visual contrast sensitivity in never-medicated, first-episode schizophrenia. *J Abnorm Psychol*. 2010;119:586-593.
7. Maekawa T, Katsuki S, Kishimoto J, et al. Altered visual information processing systems in bipolar disorder: evidence from visual MMN and P3. *Frontiers in human neuroscience*. 2013;7:403.
8. Turetsky BI, Calkins ME, Light GA, Olincy A, Radant AD, Swerdlow NR. Neurophysiological endophenotypes of schizophrenia: the viability of selected candidate measures. *Schizophrenia bulletin*. 2007;33:69-94.
9. Uhlhaas PJ, Mishara AL. Perceptual Anomalies in Schizophrenia: Integrating Phenomenology and Cognitive Neuroscience. *Schizophrenia Bulletin*. Vol 332006:142-156.
10. Butler PD, Thompson JL, Seitz AR, Deveau J, Silverstein SM. Visual perceptual remediation for individuals with schizophrenia: Rationale, method, and three case studies. *Psychiatr Rehabil J*. 2017;40:43-52.
11. Chen Y. Abnormal Visual Motion Processing in Schizophrenia: A Review of Research Progress. *Schizophrenia Bulletin*. Vol 372011:709-715.
12. Silverstein SM, Keane BP. Perceptual organization impairment in schizophrenia and associated brain mechanisms: review of research from 2005 to 2010. *Schizophrenia bulletin*. Vol 372011:690-699.
13. Tadin D, Kim J, Doop ML, et al. Weakened Center-Surround Interactions in Visual Motion Processing in Schizophrenia. *The Journal of Neuroscience*. 2006;26:11403-11412.
14. Lee J, Reavis EA, Engel SA, et al. fMRI evidence of aberrant neural adaptation for objects in schizophrenia and bipolar disorder. *Hum Brain Mapp*. 2019;40:1608-1617.
15. Silverstein SM, Berten S, Essex B, Kovács I, Susmaras T, Little DM. An fMRI examination of visual integration in schizophrenia. *J Integr Neurosci*. 2009;8:175-202.
16. Javitt DC. When doors of perception close: Bottom-up models of disrupted cognition in schizophrenia. *Annual Review of Clinical Psychology*. Vol 52009:249-275.

17. Sehatpour P, Dias EC, Butler PD, et al. Impaired Visual Object Processing Across an Occipital-Frontal-Hippocampal Brain Network in Schizophrenia. *Archives of General Psychiatry*. Vol 672010:772.
18. Butler PD, Silverstein SM, Dakin SC. Visual perception and its impairment in schizophrenia. *Biol Psychiatry*. 2008;64:40-47.
19. Cuthbert BN, Insel TR. Toward the future of psychiatric diagnosis: the seven pillars of RDoC. *BMC medicine*. 2013;11:126.
20. Insel T, Cuthbert B, Garvey M, et al. Research domain criteria (RDoC): toward a new classification framework for research on mental disorders: Am Psychiatric Assoc; 2010.
21. Dumoulin SO, Wandell BA. Population receptive field estimates in human visual cortex. *Neuroimage*. 2008;39:647-660.
22. Sereno MI, Dale AM, Reppas JB, et al. Borders of multiple visual areas in humans revealed by functional magnetic resonance imaging. *Science (New York, N.Y.)*. 1995;268:889-893.
23. Kanwisher N, Yovel G. The fusiform face area: a cortical region specialized for the perception of faces. *Philosophical Transactions of the Royal Society B: Biological Sciences*. Vol 3612006:2109-2128.
24. Rosenke M, van Hoof R, van den Hurk J, Grill-Spector K, Goebel R. A probabilistic functional atlas of human occipito-temporal visual cortex. *bioRxiv*. 2020:2020.2001.2022.916239.
25. Frost, Goebel. Measuring structural-functional correspondence: spatial variability of specialised brain regions after macro-anatomical alignment. *Neuroimage*. 2012;59:1369-1381.
26. Peters B, Kaiser J, Rahm B, Bledowski C. Activity in Human Visual and Parietal Cortex Reveals Object-Based Attention in Working Memory. *The Journal of Neuroscience*. 2015;35:3360-3369.
27. Brett M, Johnsrude IS, Owen AM. The problem of functional localization in the human brain. *Nat Rev Neurosci*. 2002;3:243-249.
28. Desai R, Liebenthal E, Possing ET, Waldron E, Binder JR. Volumetric vs. surface-based alignment for localization of auditory cortex activation. *Neuroimage*. 2005;26:1019-1029.
29. Dougherty RF, Koch VM, Brewer AA, Fischer B, Modersitzki J, Wandell BA. Visual field representations and locations of visual areas V1/2/3 in human visual cortex. *J Vis*. 2003;3:586-598.
30. Fischl B, Sereno MI, Dale AM. Cortical surface-based analysis. II: Inflation, flattening, and a surface-based coordinate system. *Neuroimage*. 1999;9:195-207.
31. Steinmetz H, Fürst G, Freund HJ. Variation of perisylvian and calcarine anatomic landmarks within stereotaxic proportional coordinates. *AJNR Am J Neuroradiol*. 1990;11:1123-1130.
32. Van Essen DC, Drury HA, Dickson J, Harwell J, Hanlon D, Anderson CH. An integrated software suite for surface-based analyses of cerebral cortex. *J Am Med Inform Assoc*. 2001;8:443-459.
33. Zilles K, Schleicher A, Langemann C, et al. Quantitative analysis of sulci in the human cerebral cortex: Development, regional heterogeneity, gender

- difference, asymmetry, intersubject variability and cortical architecture. *Human Brain Mapping*. 1997;5:218-221.
34. Bridge H. Mapping the visual brain: how and why. *Eye (Lond)*. 2011;25:291-296.
  35. Fedorenko E, Hsieh PJ, Nieto-Castañón A, Whitfield-Gabrieli S, Kanwisher N. New method for fMRI investigations of language: defining ROIs functionally in individual subjects. *J Neurophysiol*. 2010;104:1177-1194.
  36. Evans AC, Collins D, Mills SR, Brown E, Kelly R, Peters T. 3D statistical neuroanatomical models from 305 MRI volumes. *1993 IEEE Conference Record Nuclear Science Symposium and Medical Imaging Conference*. 1993:1813-1817 vol.1813.
  37. Ghosh SS, Kakunoori S, Augustinack J, et al. Evaluating the validity of volume-based and surface-based brain image registration for developmental cognitive neuroscience studies in children 4 to 11 years of age. *NeuroImage*. 2010;53:85-93.
  38. Klein A, Ghosh SS, Avants B, et al. Evaluation of volume-based and surface-based brain image registration methods. *Neuroimage*. 2010;51:214-220.
  39. Talairach J, & Tournoux, P. *Co-planar stereotaxic atlas of the human brain: 3-dimensional proportional system : an approach to cerebral imaging*. Stuttgart: Thieme; 1988.
  40. Fischl B, Sereno MI, Tootell RB, Dale AM. High-resolution intersubject averaging and a coordinate system for the cortical surface. *Hum Brain Mapp*. 1999;8:272-284.
  41. Julian JB, Fedorenko E, Webster J, Kanwisher N. An algorithmic method for functionally defining regions of interest in the ventral visual pathway. *NeuroImage*. 2012;60:2357-2364.
  42. Pantazis D, Joshi A, Jiang J, et al. Comparison of landmark-based and automatic methods for cortical surface registration. *Neuroimage*. 2010;49:2479-2493.
  43. Van Essen DC, Drury HA. Structural and functional analyses of human cerebral cortex using a surface-based atlas. *J Neurosci*. 1997;17:7079-7102.
  44. Anticevic A, Dierker DL, Gillespie SK, Csernansky JG. Comparing Surface-Based and Volume-Based Analyses of Functional Neuroimaging Data in Patients with Schizophrenia. *journal of neuroimaging*. Vol 412008:835-848.
  45. Goebel R, Esposito F, Formisano E. Analysis of functional image analysis contest (FIAC) data with brainvoyager QX: From single-subject to cortically aligned group general linear model analysis and self-organizing group independent component analysis. *Hum Brain Mapp*. 2006;27:392-401.
  46. Green MF, Kern RS, Heaton RK. Longitudinal studies of cognition and functional outcome in schizophrenia: implications for MATRICS. *Schizophr Res*. 2004;72:41-51.
  47. Harvey PD, Strassnig M. Predicting the severity of everyday functional disability in people with schizophrenia: cognitive deficits, functional capacity, symptoms, and health status. *World Psychiatry*. 2012;11:73-79.
  48. Felleman DJ, Van Essen DC. Distributed hierarchical processing in the primate cerebral cortex. *Cereb Cortex*. 1991;1:1-47.
  49. Ungerleider LG. Two cortical visual systems1982.
  50. Huff T, Mahabadi N, Tadi P. Neuroanatomy, Visual Cortex. *StatPearls*. Treasure Island (FL): StatPearls Publishing

Copyright © 2022, StatPearls Publishing LLC.; 2022.

51. Goodale M, Milner D. One brain - Two visual systems. *Psychologist*. 2006;19:660-663.
52. Adam K, Rademaker R, Serences J. *Evidence for, and challenges to, sensory recruitment models of visual working memory*2021.
53. Phylactou P, Traikapi A, Papadatou-Pastou M, Konstantinou N. Sensory recruitment in visual short-term memory: A systematic review and meta-analysis of sensory visual cortex interference using transcranial magnetic stimulation. *Psychonomic Bulletin & Review*. 2022.
54. Serences JT, Ester EF, Vogel EK, Awh E. Stimulus-Specific Delay Activity in Human Primary Visual Cortex. *Psychological Science*. 2009;20:207-214.
55. Zhao Y-J, Kay KN, Tian Y, Ku Y. Sensory Recruitment Revisited: Ipsilateral V1 Involved in Visual Working Memory. *Cerebral Cortex*. 2021;32:1470-1479.
56. Yörükc H, Santacrocce LA, Tamber-Rosenau BJ. Reevaluating the sensory recruitment model by manipulating crowding in visual working memory representations. *Psychonomic Bulletin & Review*. 2020;27:1383-1396.
57. Downing PE, Chan AW, Peelen MV, Dodds CM, Kanwisher N. Domain specificity in visual cortex. *Cereb Cortex*. 2006;16:1453-1461.
58. Kanwisher N, McDermott J, Chun MM. The fusiform face area: a module in human extrastriate cortex specialized for face perception. *J Neurosci*. 1997;17:4302-4311.
59. Kraft A, Schira MM, Hagendorf H, Schmidt S, Olma M, Brandt SA. fMRI localizer technique: efficient acquisition and functional properties of single retinotopic positions in the human visual cortex. *NeuroImage*. 2005;28:453-463.
60. Kuo BC, Nobre AC, Scerif G, Astle DE. Top-Down Activation of Spatiotopic Sensory Codes in Perceptual and Working Memory Search. *J Cogn Neurosci*. 2016;28:996-1009.
61. Linden DE, Prvulovic D, Formisano E, et al. The functional neuroanatomy of target detection: an fMRI study of visual and auditory oddball tasks. *Cereb Cortex*. 1999;9:815-823.
62. Wynn JK, Jimenez AM, Roach BJ, et al. Impaired target detection in schizophrenia and the ventral attentional network: Findings from a joint event-related potential–functional MRI analysis. *NeuroImage: Clinical*. 2015;9:95-102.
63. Bressler DW, Silver MA. Spatial attention improves reliability of fMRI retinotopic mapping signals in occipital and parietal cortex. *Neuroimage*. 2010;53:526-533.
64. Himmelberg MM, Winawer J, Carrasco M. Linking individual differences in human primary visual cortex to contrast sensitivity around the visual field. *Nat Commun*. 2022;13:3309.
65. Amunts K, Malikovic A, Mohlberg H, Schormann T, Zilles K. Brodmann's Areas 17 and 18 Brought into Stereotaxic Space—Where and How Variable? *NeuroImage*. 2000;11:66-84.
66. Uylings HBM, Rajkowska G, Sanz-Arigitia E, Amunts K, Zilles K. Consequences of large interindividual variability for human brain atlases: converging macroscopical imaging and microscopical neuroanatomy. *Anatomy and Embryology*. 2005;210:423-431.

67. Stensaas SS, Eddington DK, Dobbelle WH. The topography and variability of the primary visual cortex in man. *J Neurosurg.* 1974;40:747-755.
68. Watson JD, Myers R, Frackowiak RS, et al. Area V5 of the human brain: evidence from a combined study using positron emission tomography and magnetic resonance imaging. *Cereb Cortex.* 1993;3:79-94.
69. Schwarzkopf DS, Robertson DJ, Song C, Barnes GR, Rees G. The Frequency of Visually Induced Gamma-Band Oscillations Depends on the Size of Early Human Visual Cortex. *The Journal of Neuroscience.* 2012;32:1507-1512.
70. Zhang J, Cheng W, Liu Z, et al. Neural, electrophysiological and anatomical basis of brain-network variability and its characteristic changes in mental disorders. *Brain.* 2016;139:2307-2321.
71. Anderson J, Cameron E, Levine M. A method for quantifying visual field inhomogeneities. *Vision Research.* 2014;105.
72. O'Connell C, Ho LC, Murphy MC, et al. Structural and functional correlates of visual field asymmetry in the human brain by diffusion kurtosis MRI and functional MRI. *Neuroreport.* 2016;27:1225-1231.
73. Poldrack RA, Mumford JA, Nichols TE. *Handbook of Functional MRI Data Analysis.* Cambridge: Cambridge University Press; 2011.
74. Nieto-Castanon A, Ghosh SS, Tourville JA, Guenther FH. Region of interest based analysis of functional imaging data. *Neuroimage.* 2003;19:1303-1316.
75. Blazejewska AI, Fischl B, Wald LL, Polimeni JR. Intracortical smoothing of small-voxel fMRI data can provide increased detection power without spatial resolution losses compared to conventional large-voxel fMRI data. *Neuroimage.* 2019;189:601-614.
76. Kay K, Jamison KW, Vizioli L, Zhang R, Margalit E, Ugurbil K. A critical assessment of data quality and venous effects in sub-millimeter fMRI. *Neuroimage.* 2019;189:847-869.
77. Fischl B, Rajendran N, Busa E, et al. Cortical folding patterns and predicting cytoarchitecture. *Cereb Cortex.* 2008;18:1973-1980.
78. Hinds OP, Rajendran N, Polimeni JR, et al. Accurate prediction of V1 location from cortical folds in a surface coordinate system. *NeuroImage.* 2008;39:1585-1599.
79. Huang T, Chen X, Jiang J, Zhen Z, Liu J. A probabilistic atlas of the human motion complex built from large-scale functional localizer data. *Hum Brain Mapp.* 2019;40:3475-3487.
80. Weiner KS, Barnett MA, Witthoft N, et al. Defining the most probable location of the parahippocampal place area using cortex-based alignment and cross-validation. *Neuroimage.* 2018;170:373-384.
81. Wang L, Mruczek RE, Arcaro MJ, Kastner S. Probabilistic Maps of Visual Topography in Human Cortex. *Cereb Cortex.* 2015;25:3911-3931.
82. Yamamoto H, Fukunaga M, Takahashi S, et al. Inconsistency and uncertainty of the human visual area loci following surface-based registration: Probability and Entropy Maps. *Hum Brain Mapp.* 2012;33:121-129.
83. Chen H, Yao D, Liu Z. A study on asymmetry of spatial visual field by analysis of the fMRI BOLD response. *Brain Topogr.* 2004;17:39-46.

84. Loughnane GM, Shanley JP, Lalor EC, O'Connell RG. Behavioral and electrophysiological evidence of opposing lateral visuospatial asymmetries in the upper and lower visual fields. *Cortex*. 2015;63:220-231.
85. Curcio CA, Allen KA. Topography of ganglion cells in human retina. *J Comp Neurol*. 1990;300:5-25.
86. Eickhoff SB, Rottschy C, Kujovic M, Palomero-Gallagher N, Zilles K. Organizational Principles of Human Visual Cortex Revealed by Receptor Mapping. *Cerebral Cortex*. 2008;18:2637-2645.
87. Silson EH, Reynolds RC, Kravitz DJ, Baker CI. Differential Sampling of Visual Space in Ventral and Dorsal Early Visual Cortex. *The Journal of Neuroscience*. 2018;38:2294-2303.
88. Hagler DJ, Jr. Visual field asymmetries in visual evoked responses. *J Vis*. 2014;14:13.
89. Rubin N, Nakayama K, Shapley R. Enhanced perception of illusory contours in the lower versus upper visual hemifields. *Science*. 1996;271:651-653.
90. Schmidtman G, Logan AJ, Kennedy GJ, Gordon GE, Loffler G. Distinct lower visual field preference for object shape. *J Vis*. 2015;15:18.
91. Thomas NA, Elias LJ. Upper and lower visual field differences in perceptual asymmetries. *Brain Res*. 2011;1387:108-115.
92. Brodoehl S, Gaser C, Dahnke R, Witte OW, Klingner CM. Surface-based analysis increases the specificity of cortical activation patterns and connectivity results. *Scientific Reports*. 2020;10:5737.
93. Bullmore E, Sporns O. Complex brain networks: graph theoretical analysis of structural and functional systems. *Nature Reviews Neuroscience*. 2009;10:186-198.
94. Yang Z, Fang F, Weng X. Recent developments in multivariate pattern analysis for functional MRI. *Neurosci Bull*. 2012;28:399-408.
95. Haxby JV, Gobbini MI, Furey ML, Ishai A, Schouten JL, Pietrini P. Distributed and overlapping representations of faces and objects in ventral temporal cortex. *Science*. 2001;293:2425-2430.
96. Coutanche MN, Thompson-Schill SL, Schultz RT. Multi-voxel pattern analysis of fMRI data predicts clinical symptom severity. *NeuroImage*. 2011;57:113-123.
97. Bleich-Cohen M, Jamsky S, Sharon H, et al. Machine learning fMRI classifier delineates subgroups of schizophrenia patients. *Schizophrenia Research*. 2014;160:196-200.
98. Zeng LL, Shen H, Liu L, et al. Identifying major depression using whole-brain functional connectivity: a multivariate pattern analysis. *Brain*. 2012;135:1498-1507.
99. Conroy BR, Singer BD, Guntupalli JS, Ramadge PJ, Haxby JV. Inter-subject alignment of human cortical anatomy using functional connectivity. *NeuroImage*. 2013;81:400-411.
100. Frost, Goebel. Functionally informed cortex based alignment: an integrated approach for whole-cortex macro-anatomical and ROI-based functional alignment. *NeuroImage*. 2013;83:1002-1010.
101. Sabuncu MR, Singer BD, Conroy B, Bryan RE, Ramadge PJ, Haxby JV. Function-based Intersubject Alignment of Human Cortical Anatomy. *Cerebral Cortex*. 2009;20:130-140.



102. Conroy BR, Singer BD, Haxby JV, Ramadge PJ. fMRI-Based Inter-Subject Cortical Alignment Using Functional Connectivity. *Adv Neural Inf Process Syst*. 2009;22:378-386.
103. Rademacher J, Caviness VS, Jr., Steinmetz H, Galaburda AM. Topographical variation of the human primary cortices: implications for neuroimaging, brain mapping, and neurobiology. *Cereb Cortex*. 1993;3:313-329.
104. Glasser MF, Coalson TS, Robinson EC, et al. A multi-modal parcellation of human cerebral cortex. *Nature*. 2016;536:171-178.
105. Manoach DS. Prefrontal cortex dysfunction during working memory performance in schizophrenia: reconciling discrepant findings. *Schizophr Res*. 2003;60:285-298.
106. Bakroon A, Lakshminarayanan V. Visual function in autism spectrum disorders: a critical review. *Clin Exp Optom*. 2016;99:297-308.
107. Butler PD, Schechter I, Zemon V, et al. Dysfunction of early-stage visual processing in schizophrenia. *Am J Psychiatry*. 2001;158:1126-1133.
108. Chen CY, Chen CL, Wu CY, Chen HC, Tang FT, Wong MK. Visual spatial attention in children with attention deficit hyperactivity disorder. *Chang Gung Med J*. 2002;25:514-521.
109. Hale TS, Kane AM, Kaminsky O, et al. Visual Network Asymmetry and Default Mode Network Function in ADHD: An fMRI Study. *Front Psychiatry*. 2014;5:81.
110. Sanz-Cervera P, Pastor-Cerezuela G, González-Sala F, Tárraga-Mínguez R, Fernández-Andrés M-I. Sensory Processing in Children with Autism Spectrum Disorder and/or Attention Deficit Hyperactivity Disorder in the Home and Classroom Contexts. *Front Psychol*. 2017;8:1772-1772.
111. Seymour RA, Rippon G, Gooding-Williams G, Schoffelen JM, Kessler K. Dysregulated oscillatory connectivity in the visual system in autism spectrum disorder. *Brain*. 2019;142:3294-3305.
112. Shimizu VT, Bueno OF, Miranda MC. Sensory processing abilities of children with ADHD. *Braz J Phys Ther*. 2014;18:343-352.
113. Deng Y, Liu K, Cheng D, et al. Ventral and dorsal visual pathways exhibit abnormalities of static and dynamic connectivities, respectively, in patients with schizophrenia. *Schizophrenia research*. 2019;206:103-110.
114. Plomp G, Roinishvili M, Chkonia E, et al. Electrophysiological Evidence for Ventral Stream Deficits in Schizophrenia Patients. *Schizophrenia Bulletin*. 2013;39:547-554.
115. Tek C, Gold J, Blaxton T, Wilk C, McMahan RP, Buchanan RW. Visual Perceptual and Working Memory Impairments in Schizophrenia. *Archives of general psychiatry*. 2002;59:146.
116. Hettwer MD, Lancaster TM, Raspor E, et al. Evidence From Imaging Resilience Genetics for a Protective Mechanism Against Schizophrenia in the Ventral Visual Pathway. *Schizophrenia Bulletin*. 2022;48:551-562.

## **Schriftliche Erklärung**

Ich erkläre ehrenwörtlich, dass ich die dem Fachbereich Medizin der Johann Wolfgang Goethe-Universität Frankfurt am Main zur Promotionsprüfung eingereichte Dissertation mit dem Titel

Improved correspondence of fMRI visual field localizer data after cortex-based macroanatomical alignment

am Zentrum der Psychischen Gesundheit, Klinik für Psychiatrie, Psychosomatik und Psychotherapie, unter Betreuung und Anleitung von Prof. Dr. Andreas Reif mit Unterstützung durch Dr. Robert Bittner ohne sonstige Hilfe selbst durchgeführt und bei der Abfassung der Arbeit keine anderen als die in der Dissertation angeführten Hilfsmittel benutzt habe. Darüber hinaus versichere ich, nicht die Hilfe einer kommerziellen Promotionsvermittlung in Anspruch genommen zu haben.

Ich habe bisher an keiner in- oder ausländischen Universität ein Gesuch um Zulassung zur Promotion eingereicht\*. Die vorliegende Arbeit wurde bisher nicht als Dissertation eingereicht.

Vorliegende Ergebnisse der Arbeit wurden (oder werden) in folgendem Publikationsorgan veröffentlicht:

Qubad, Mishal; Barnes-Scheufler, Catherine Victoria; Schaum, Michael; Raspor, Eva; Peters, Benjamin; Rösler, Lara; Goebel, Rainer; Reif, Andreas; Bittner, Robert Arthur. Improved correspondence of fMRI visual field localizer data after cortex-based macroanatomical alignment. Scientific Reports. 2022 Aug 22;12:14310

---

(Ort, Datum)

---

(Unterschrift)

\*) im Falle des Nichtzutreffens entfernen

## Danksagung

[Redacted]

[Redacted]

[Redacted]

[Redacted]

[Redacted]

Name/Vorname: Qubad, Mishal  
Geburtsdatum: 29.08.1989


## Schriftliche Erklärung

Nach bestandener Doktorprüfung lege ich hiermit die Bescheinigung der Universitätsbibliothek über die Abgabe der erforderlichen Pflichtexemplare meiner Dissertation sowie die Pflichtexemplare meiner Dissertation für das Dekanat vor.

Diese Pflichtexemplare lege ich in der Version vor, die auch den Gutachtern (Referent, Korreferent/en) im Promotionsverfahren vorgelegen hat. Ich versichere mit meiner Unterschrift, dass ich außer den Ergänzungen

- zum/ zu den Korreferenten,
- dem Tag der mündlichen Prüfung

auf der Seite 2 meiner Dissertation keine Änderungen vorgenommen habe.

04.05.2023   

---

(Datum, Unterschrift)